

Anil Misra · Viraj Singh

# Thermomechanics-based nonlinear rate-dependent coupled damage-plasticity granular micromechanics model

Received: 17 December 2013 / Accepted: 20 April 2014 / Published online: 11 May 2014  
© Springer-Verlag Berlin Heidelberg 2014

**Abstract** Thermomechanics and granular micromechanics approaches are combined to derive constitutive equations for modeling rate-dependent granular materials with damage and plasticity. The derivation is motivated by the recognition that the effect of micro-scale mechanisms upon the macro-scale behavior is known to be significant for granular materials. A general thermomechanical framework applicable to rate-dependent granular materials with damage and plasticity is developed. Based upon this framework, an expression for macro-scale Cauchy stress tensor is obtained in terms of the micro-scale grain interaction forces and the relationship between micro- and macro-scale kinematics. In addition, a Clausius–Duhem type inequality applicable to inter-granular interaction is derived, which is used to establish micro-scale constitutive relations for particular type of inter-granular interactions. The expression for Cauchy stress tensor and the micro-scale constitutive relations is then combined under a mean field kinematic assumption to obtain evolution-type macro-scale constitutive equations. The advantage of the granular micromechanics approach is that the damage and plasticity are defined using simple 1d functions at micro-scale, and complicated plastic potentials, damage functions and rules for their evolution are not required. The resultant model is applied to investigate primary, secondary and tertiary creep, creep-recovery as well as rate-dependent response under uniaxial compressive loading. Model applicability is also demonstrated for asymmetric tensile-compressive response under creep-recovery loading. The model is used to evaluate the evolution of elastic energy, and viscous, plastic and damage dissipation at the macro- and micro-scale with respect to creep time and loading level. The results show the development of loading-induced anisotropy due to damage and plasticity in these materials.

**Keywords** Thermomechanics · Rate dependence · Damage-plasticity · Granular materials · Micromechanics · Time integration

## 1 Introduction

A large class of materials possessing granular microstructure, such as asphalt concrete, soils, polymers, exhibit rate-dependent mechanical behavior often coupled with nonlinear material damage. Although a number of constitutive models have been proposed in the literature to model nonlinear viscoelastic behavior (see for

---

Communicated by Francesco dell’Isola and Giuseppe Piccardo.

A. Misra (✉)  
Civil, Environmental and Architectural Engineering Department, University of Kansas, 1530 W. 15th Street, Learned Hall,  
Lawrence, KS 66045-7609, USA  
E-mail: amisra@ku.edu  
Tel.: (785)-864-1750  
Fax: (785)-864-5631

V. Singh  
Mechanical Engineering Department, University of Kansas, 1530 W. 15th Street, Learned Hall, Lawrence, KS 66045-7609, USA

example [1–9] including comprehensive reviews in [2,6]), these efforts characteristically focus upon the macro-scale without adequate considerations of the micro-scale mechanisms that are known to be significant for granular materials. The granular micromechanics approach provides a feasible method for incorporating the influence of micro-scale mechanisms into continuum models of these materials [10]. The recognition that microstructural effects are significant and can be modeled within the framework of continuum mechanics can be traced to the pioneering works of Cosserat [11], Mindlin [12], Toupin [13], Eringen [14], Green and Rivlin [15] and Germain [16]. The granular micromechanics approach traces its genesis to the continuum models of grain packings developed in the second half of the last century (see for example [17–23]). However, this approach has antecedents in the early development of continuum mechanics in the works of Navier [24], Cauchy [25], and Piola [26]. In recent years, approaches have been sought to obtain continuum model of discrete systems such as for molecular or atomic systems [27–29], granular systems [30–35], truss-systems [36–38] or for modeling fracture assuming a pseudo-granular structure [39–41]. Thermomechanics can serve as a basis for the development of granular micromechanics or similar approaches for nonlinear rate-dependent materials with damage and plasticity that is thermodynamically consistent [6,42–45]. The focus of the present paper is to discuss the derivation of continuum constitutive relationships using granular micromechanics approach from a thermomechanical basis.

In the subsequent discussion, we first develop the general thermomechanical framework applicable to rate-dependent granular materials with coupled damage-plasticity. As a result, we derive an expression for macro-scale Cauchy stress tensor in terms of the micro-scale grain interaction forces and the relationship between micro- and macro-scale kinematics. We also find a Clausius–Duhem type inequality applicable to inter-granular interactions. We then derive micro-scale constitutive relations for particular type of inter-granular interactions. These micro-scale constitutive relations are used along with the expression for Cauchy stress to find the macro-scale constitutive relationship. For numerical calculations, an efficient and accurate explicit time integration scheme for the resultant evolution-type macro-scale constitutive equations is derived. The model is then applied to investigate primary, secondary and tertiary creep, creep-recovery and rate-dependent response under uniaxial compressive and tensile loading. We first demonstrate the model validity by comparison with experimental data from creep and creep-recovery test of hot-mix asphalt samples under both compressive and tensile loading. We then evaluate the evolution of elastic energy, and viscous, plastic and damage dissipation at the macro- and micro-scale with respect to creep time and loading level. We also investigate how damage and plastic displacement evolve during creep, creep-recovery and monotonic loading. These results are discussed in context of the strong loading-induced anisotropy that these materials exhibit. The model is also applied to simulate nonlinear rate-dependent bending experiments on polymeric beams.

## 2 Thermomechanical framework for granular micromechanics

It is well accepted that the macro-scale properties of a material are significantly influenced by the interaction between representative units. In many systems, the relevant representative unit can be modeled as grains conceived as aggregations of atoms or molecules in which the intra-granular atomic interactions have a qualitatively different nature than the inter-granular interactions. Some materials such grains are easily identifiable with distinct grain boundaries, such as in the cases of grain packings, polycrystals, sands and clays, asphalt concrete, sandstones or materials derived from sintering using grain precursors. In contrast, for a number of materials with granular texture or behavior, the grain identification is not straightforward, such as the case of hydraulic cements and polymers. In either case, the evidence of granular nature (and grain size) of materials and the ideas of coarse graining by combining atoms and molecules into larger grains have been prevalent (see for example [46–50]). In these cases, a granular meso-structure is considered and the inter-granular interactions modeled in a statistical sense to describe the essential grain scale and sub-granular scale mechanisms. In principle, the inter-granular interaction in a grain neighborhood may be treated from atomistic viewpoint; however, such an approach can be computationally intractable for most systems with billions of atoms and ill-defined structures. Along these lines, multi-scale approaches that consider intermediate or meso-scale consisting of discrete grains could also be conceived. However, these discrete models suffer from the need to simulate granular meso-structures, define appropriate grain scale constitutive laws, implement effective computational schemes and be coupled to higher scales. Such intermediate scale discrete models not only add to the computational expense, but fail to offer the versatility of systematically investigating the influence of the macro-scale parameters, such as material density and inherent anisotropy, as well as the grain scale parameters, such as effect of inter-granular degradation, presence of boundary layers, shapes and sizes, on the overall material response. From a practical viewpoint, we can formulate appropriate functions to describe the inter-granular interactions

in which the essential grain scale mechanisms are represented and the interaction function parameters can be obtained from the experimental data. Therefore, in this paper, we proceed from a pseudo-granular structure in which the grain interactions represent the average behavior of a variety of plausible inter-atomic interactions and the influence of the grain neighborhood.

## 2.1 Kinematics of granular meso-structure

Under external action, the grains of the meso-structure may translate or rotate resulting in a relative displacement between the grains [18,34]. As a first approximation, we ignore the grain rotations and write the relative displacement,  $\delta_i$ , between two nearest neighbor grains  $n$  and  $p$  as

$$\delta_i = u_i^p - u_i^n \quad (1)$$

where  $u_i$  = particle displacement; superscripts refer to the interacting particles. The subscripts follow the tensor summation convention unless noted otherwise. For passage to continuum description of this discrete model, we utilize the Taylor series expansion of the displacement such that the displacement of grain  $p$  may be written as:

$$u_i^p = u_i^n + u_{i,j}^n (x_j^p - x_j^n) \quad (2)$$

where the point of expansion is chosen as the centroid of grain  $n$ . In Eq. 2,  $u_{i,j}$  is the displacement gradient, and  $x_j^n$  and  $x_j^p$  are the position vectors to the centroid of grains  $n$  and  $p$ , respectively. Thus, the relative displacement,  $\delta_i$ , between two nearest neighbor grains  $n$  and  $p$  representing the  $\alpha$ -th inter-granular interaction is given by

$$\delta_i^\alpha = u_{i,j}^n (x_j^p - x_j^n) = u_{i,j}^n l_j^\alpha \quad (3)$$

The relative displacement,  $\delta_i$ , between two grains may be decomposed into two components, (1)  $\delta_n$ , along unit vector,  $n_i$ , defined in the direction of vector  $l_j^\alpha = x_j^p - x_j^n$ , termed as the normal direction, and (2)  $\delta_w$ , orthogonal to vector,  $n_i$ , referred to as shear direction. The relative displacement in the normal direction is given by,  $\delta_n = \delta_i n_i$ , and the relative displacement in the shear direction is given by,  $\delta_w = \sqrt{(\delta_i s_i)^2 + (\delta_i t_i)^2}$ , where unit vectors  $n_i$ ,  $s_i$  and  $t_i$  form a local Cartesian coordinate system. The vectors  $s_i$  and  $t_i$  are arbitrarily chosen and lie on the plane perpendicular to the vector  $n_i$ , such that

$$\begin{aligned} n_i &= \langle \cos \theta, \sin \theta \cos \phi, \sin \theta \sin \phi \rangle \\ s_i &= \langle -\sin \theta, \cos \theta \cos \phi, \cos \theta \sin \phi \rangle \\ t_i &= \langle 0, -\sin \phi, \cos \phi \rangle \end{aligned} \quad (4)$$

where  $\theta$  and  $\phi$  are shown in the inset in Fig. 3. We note here that the above simplifying kinematical assumptions that ignore the particle rotations and higher gradients of displacements will lead to a classical Cauchy continuum theory, albeit with grain scale representation. By relaxing these assumptions, continuum theories that provide a much more complete account of microstructure such as those discussed in [51–54] may be obtained. However, this requires a careful kinematical analysis that will be pursued in a future work.

## 2.2 Thermomechanical formulation for rate-dependent material with damage

To establish our notations, we consider a volume element (VE) of granular material with mass density denoted by,  $\rho$ . Using the first law of thermodynamics, which states that the change in the total energy (kinetic and internal) of the system is equal to amount of work done on the system and heat supplied to the system, the variation of internal energy density of the VE is written as the following sum

$$\rho \dot{e} = p^i - q_{k,k} + \rho h \quad (5)$$

where  $e$  is the internal energy per unit mass,  $p^i$  is the power density of internal forces,  $q_k$  is the heat flux vector and  $h$  is the heat source per unit mass. Further, the second law of thermodynamics, which states that the change

of entropy of the system is greater than or equal to the supply of entropy through heat, provides the following inequality

$$\rho\theta\dot{s} - \rho h + q_{k,k} - \frac{q_k\theta_{,k}}{\theta} \geq 0 \quad (6)$$

where  $s$  is the entropy per unit mass, and  $\theta$  is the thermodynamic temperature. Making use of Helmholtz free energy per unit mass,  $w$ , expressed as a Legendre transform

$$w = e - s\theta \quad (7)$$

Equation 5 can be written as

$$\rho\theta\dot{s} = p^i - q_{k,k} + \rho h - \rho\dot{\theta}s - \rho\dot{w} \quad (8)$$

Now combining Eqs. 6 and 8, we obtain the well-known Clausius–Duhem inequality

$$p^i - \rho\dot{w} - \rho\dot{\theta}s - \frac{q_k\theta_{,k}}{\theta} \geq 0 \quad (9)$$

For small deformation, Helmholtz free energy and entropy per unit volume may be defined as:  $W = \rho w$  and  $S = \rho s$ , and the following usable form of Clausius–Duhem inequality can be obtained

$$p^i - \dot{W} - S\dot{\theta} - \frac{q_k\theta_{,k}}{\theta} = d \geq 0 \quad (10)$$

where  $d$  denotes the dissipation per unit volume [55].

For further discussion, we assume that the power density of internal forces,  $p^i$ , is a function of the symmetric part of first gradient of displacement, that is  $p^i = \sigma_{ij}\dot{u}_{(i,j)} = \sigma_{ij}\dot{\varepsilon}_{ij}$ , where  $\sigma_{ij}$  is the Cauchy stress. In general, the power density of internal forces could be a function of higher gradients of displacements as well as rotations which would lead to higher gradient and micromorphic materials (see [16, 56, 57]). The Helmholtz free energy density of rate-dependent material with damage is taken to be a function of the independent kinematic variable,  $\varepsilon_{ij}$ ; the internal variable associated with rate-dependent phenomenon,  $\varepsilon_{ij}^v$ ; a second internal variable associated with damage,  $D_{ij}$ ; a third internal variable associated with plasticity,  $\varepsilon_{ij}^p$ ; and the temperature,  $\theta$ , expressed in the following general form:  $W = W(\varepsilon_{ij}, \varepsilon_{ij}^v, D_{ij}, \varepsilon_{ij}^p, \theta)$ . In addition, the dissipation density,  $d$ , is defined as

$$d = \frac{\partial\psi}{\partial\dot{\varepsilon}_{ij}^v}\dot{\varepsilon}_{ij}^v + \frac{\partial\psi}{\partial\dot{\varepsilon}_{ij}^p}\dot{\varepsilon}_{ij}^p + \frac{\partial\psi}{\partial\dot{D}_{ij}}\dot{D}_{ij} + \frac{\partial\psi}{\partial q_k}q_k \geq 0 \quad (11)$$

where,  $\psi = \psi(\varepsilon_{ij}, \theta, \varepsilon_{ij}^v, \dot{\varepsilon}_{ij}^v, D_{ij}, \dot{D}_{ij}, q_k)$  is a dissipation potential. Differentiating the Helmholtz free energy,  $W$ , with time we obtain

$$\dot{W} = \frac{\partial W}{\partial\varepsilon_{ij}}\dot{\varepsilon}_{ij} + \frac{\partial W}{\partial\varepsilon_{ij}^v}\dot{\varepsilon}_{ij}^v + \frac{\partial W}{\partial\varepsilon_{ij}^p}\dot{\varepsilon}_{ij}^p + \frac{\partial W}{\partial D_{ij}}\dot{D}_{ij} + \frac{\partial W}{\partial\theta}\dot{\theta} \quad (12)$$

Combining Eqs. 10, 11 and 12, we obtain the following

$$\begin{aligned} & \left(\sigma_{ij} - \frac{\partial W}{\partial\varepsilon_{ij}}\right)\dot{\varepsilon}_{ij} - \left(\frac{\partial W}{\partial\varepsilon_{ij}^v} + \frac{\partial\psi}{\partial\dot{\varepsilon}_{ij}^v}\right)\dot{\varepsilon}_{ij}^v - \left(\frac{\partial W}{\partial\varepsilon_{ij}^p} + \frac{\partial\psi}{\partial\dot{\varepsilon}_{ij}^p}\right)\dot{\varepsilon}_{ij}^p \\ & - \left(\frac{\partial W}{\partial D_{ij}} + \frac{\partial\psi}{\partial\dot{D}_{ij}}\right)\dot{D}_{ij} - \left(\frac{\partial W}{\partial\theta} + S\right)\dot{\theta} - \left(\frac{\theta_{,k}}{\theta} + \frac{\partial\psi}{\partial q_k}\right)q_k = 0 \end{aligned} \quad (13)$$

For Eq. 13 to hold under all conditions, the following must be satisfied

$$\sigma_{ij} - \frac{\partial W}{\partial \varepsilon_{ij}} = 0 \quad (14a)$$

$$\frac{\partial W}{\partial \varepsilon_{ij}^v} + \frac{\partial \psi}{\partial \dot{\varepsilon}_{ij}^v} = 0 \quad (14b)$$

$$\frac{\partial W}{\partial \varepsilon_{ij}^p} + \frac{\partial \psi}{\partial \dot{\varepsilon}_{ij}^p} = 0 \quad (14c)$$

$$\frac{\partial W}{\partial D_{ij}} + \frac{\partial \psi}{\partial \dot{D}_{ij}} = 0 \quad (14d)$$

$$\frac{\partial W}{\partial \theta} + S = 0 \quad (14e)$$

$$-\frac{\theta_{,k}}{\theta} = \frac{\partial \psi}{\partial q_k} \quad (14f)$$

Clearly, Eq. 14a provides the definition of the Cauchy stress as  $\sigma_{ij} = \frac{\partial W}{\partial \varepsilon_{ij}}$ , Eqs. 14b through 14d represent Ziegler's orthogonality conditions, Eq. 14e provides the relationship between free energy and entropy  $S$ , and Eq. 14f represents the temperature gradient per unit temperature  $\frac{\theta_{,k}}{\theta}$  as a function of heat vector  $q_k$ .

### 2.3 Thermomechanical formulation for granular system

We observe that for a granular system, the VE free energy, dissipation potential and temperature may be defined in terms of the micro-scale quantities arising from the inter-granular interactions. Thus, the Helmholtz free energy density,  $W$ , and the dissipation potential,  $\Psi$ , can be written as follows:

$$W = \frac{1}{V} \sum_{\alpha}^N W^{\alpha} \left( \delta_j^{\alpha}, \delta_j^{v\alpha}, \delta_j^{p\alpha}, D_j^{\alpha}, \theta^{\alpha} \right) \quad (15a)$$

$$\psi = \frac{1}{V} \sum_{\alpha=1}^N \psi^{\alpha} \left( \delta_j^{\alpha}, \delta_j^{v\alpha}, \dot{\delta}_j^{v\alpha}, \delta_j^{p\alpha}, \dot{\delta}_j^{p\alpha}, D_j^{\alpha}, \dot{D}_j^{\alpha}, \theta^{\alpha}, q_j^{\alpha} \right) \quad (15b)$$

where each inter-granular interactions have been counted only once such that  $N$  is the total number of inter-granular interactions,  $W^{\alpha}$  and  $\psi^{\alpha}$  denote the contributions to free energy and dissipation potential, respectively, from the  $\alpha$ -th inter-granular interaction, and  $\delta_j^{\alpha}$  is the inter-granular displacement vector defined in Eq. 1,  $\delta_j^{v\alpha}$ ,  $\delta_j^{p\alpha}$  and  $D_j^{\alpha}$  are the internal variables associated with rate dependence, plasticity and damage, respectively, of the inter-granular interactions, and the superimposed dot ( $\dot{\cdot}$ ) denotes the time derivative. Similarly, the VE temperature,  $\theta$ , can be obtained as a volume average of the micro-scale temperatures associated with granular interactions,  $\theta^{\alpha}$ , as

$$\theta = \sum_{\alpha=1}^N \varphi^{\alpha} \theta^{\alpha} \quad (15c)$$

where  $\varphi^{\alpha}$  denotes the volume fraction ascribed to the  $\alpha$ -th inter-granular interactions.

Now, from Eqs. 14a and 15a, we obtain the following relationship between the macro-scale Cauchy stress,  $\sigma_{ij}$ , of the VE and the micro-scale grain interaction forces,  $f_j^{\alpha}$ , using the chain rule of differentiation

$$\sigma_{ij} = \frac{\partial W}{\partial \varepsilon_{ij}} = \frac{1}{V} \sum_{\alpha=1}^N f_k^{\alpha} \frac{\partial \delta_k^{\alpha}}{\partial \varepsilon_{ij}} \quad \text{where, } f_k^{\alpha} = \frac{\partial W^{\alpha}}{\partial \delta_k^{\alpha}} \quad (16)$$

It is noteworthy that the grain interaction forces,  $f_j^{\alpha}$ , are in general a function of the micro-scale temperature. Thus, the change in macro-scale stress could also result from micro-scale thermal expansion or contraction

caused by temperature change. A somewhat simpler form of similar expression for Cauchy stress tensor has been derived previously using alternative approaches (see [17] and more recently [58]), where a particular mean field relationship between inter-granular displacement vector and strain tensor has been tacitly assumed and dependence on temperature ignored. Further, we substitute Eqs. 15a and 15b into the Ziegler's orthogonality conditions given in Eqs. 14b–14d, use the chain rule and recognize that the variation in time of the micro-scale quantities is not independent of the macro-scale quantities. As a result, we obtain the following relationships:

$$\sum_{\alpha=1}^N \frac{\partial W^\alpha}{\partial \delta_k^{v\alpha}} \frac{\partial \delta_k^{v\alpha}}{\partial \varepsilon_{ij}^v} + \sum_{\alpha=1}^N \frac{\partial \psi^\alpha}{\partial \dot{\delta}_k^{v\alpha}} \frac{\partial \dot{\delta}_k^{v\alpha}}{\partial \dot{\varepsilon}_{ij}^v} = \sum_{\alpha=1}^N \left( \frac{\partial W^\alpha}{\partial \delta_k^{v\alpha}} + \frac{\partial \psi^\alpha}{\partial \dot{\delta}_k^{v\alpha}} \right) \frac{\partial \delta_k^{v\alpha}}{\partial \varepsilon_{ij}^v} = 0 \quad (17a)$$

$$\sum_{\alpha=1}^N \frac{\partial W^\alpha}{\partial \delta_k^{p\alpha}} \frac{\partial \delta_k^{p\alpha}}{\partial \varepsilon_{ij}^p} + \sum_{\alpha=1}^N \frac{\partial \psi^\alpha}{\partial \dot{\delta}_k^{p\alpha}} \frac{\partial \dot{\delta}_k^{p\alpha}}{\partial \dot{\varepsilon}_{ij}^p} = \sum_{\alpha=1}^N \left( \frac{\partial W^\alpha}{\partial \delta_k^{p\alpha}} + \frac{\partial \psi^\alpha}{\partial \dot{\delta}_k^{p\alpha}} \right) \frac{\partial \delta_k^{p\alpha}}{\partial \varepsilon_{ij}^p} = 0 \quad (17b)$$

$$\sum_{\alpha=1}^N \frac{\partial W^\alpha}{\partial D_k^\alpha} \frac{\partial D_k^\alpha}{\partial D_{ij}} + \sum_{\alpha=1}^N \frac{\partial \psi^\alpha}{\partial \dot{D}_k^\alpha} \frac{\partial \dot{D}_k^\alpha}{\partial \dot{D}_{ij}} = \sum_{\alpha=1}^N \left( \frac{\partial W^\alpha}{\partial D_k^\alpha} + \frac{\partial \psi^\alpha}{\partial \dot{D}_k^\alpha} \right) \frac{\partial D_k^\alpha}{\partial D_{ij}} = 0 \quad (17c)$$

The use of Eqs. 15a and 14e provides

$$\sum_{\alpha=1}^N \frac{1}{\varphi^\alpha} \frac{\partial W^\alpha}{\partial \theta^\alpha} + \sum_{\alpha=1}^N S^\alpha = 0 \quad (17d)$$

where the entropy per unit volume,  $S = \frac{1}{V} \sum_{\alpha=1}^N S^\alpha$ . And finally, from the combination of Eqs. 15c and 14f, we find the relationship between the micro-scale heat vectors and macro-scale temperature gradient

$$\sum_{\alpha=1}^N -\frac{\varphi^\alpha \theta_{,k}^\alpha}{\theta} = \sum_{\alpha=1}^N \frac{\partial \psi^\alpha}{\partial q_l^\alpha} \frac{\partial q_l^\alpha}{\partial q_k} \quad (17e)$$

An examination of Eq. 17 suggests that the following form of micro-scale Clausius–Duhem type inequality should hold for the  $\alpha$ -th inter-granular interaction:

$$f_j^\alpha \dot{\delta}_j^\alpha - \dot{W}^\alpha - \varphi^\alpha S^\alpha \dot{\theta}^\alpha - \varphi^\alpha \frac{q_k^\alpha \theta_{,k}^\alpha}{\theta} = d^\alpha \geq 0 \quad (18)$$

where,  $f_j^\alpha$ ,  $\delta_j^\alpha$  are the inter-granular force and displacements,  $W^\alpha$ ,  $S^\alpha$ ,  $d^\alpha$  and  $\varphi^\alpha \frac{q_k^\alpha \theta_{,k}^\alpha}{\theta}$  are the free energy, entropy, total dissipation and thermal dissipation, respectively, contributed by the  $\alpha$ -th inter-granular interaction, and  $q_k^\alpha$  is the heat vector associated with the  $\alpha$ -th inter-granular interaction. The dissipation,  $d^\alpha$ , is given as follows:

$$d^\alpha = \frac{\partial \psi^\alpha}{\partial \dot{\delta}_j^{v\alpha}} \dot{\delta}_j^{v\alpha} + \frac{\partial \psi^\alpha}{\partial \dot{\delta}_j^{p\alpha}} \dot{\delta}_j^{p\alpha} + \frac{\partial \psi^\alpha}{\partial \dot{D}_j^\alpha} \dot{D}_j^\alpha + \frac{\partial \psi^\alpha}{\partial q_j^\alpha} q_j^\alpha \geq 0 \quad (19)$$

where  $\psi^\alpha$ , is the micro-scale dissipation potential defined in Eq. 15b. Differentiating free energy,  $W^\alpha$ , defined in Eq. 15a with time we obtain:

$$\dot{W}^\alpha = \frac{\partial W^\alpha}{\partial \delta_j^\alpha} \dot{\delta}_j^\alpha + \frac{\partial W^\alpha}{\partial \delta_j^{v\alpha}} \dot{\delta}_j^{v\alpha} + \frac{\partial W^\alpha}{\partial \delta_j^{p\alpha}} \dot{\delta}_j^{p\alpha} + \frac{\partial W^\alpha}{\partial D_j^\alpha} \dot{D}_j^\alpha + \frac{\partial W^\alpha}{\partial \theta_j^\alpha} \dot{\theta}_j^\alpha \quad (20)$$

Now combining with Eqs. 18, 19 and 20, we obtain the following expression:

$$\begin{aligned} & \left( f_j^\alpha - \frac{\partial W^\alpha}{\partial \delta_j^\alpha} \right) \dot{\delta}_j^\alpha - \left( \frac{\partial W^\alpha}{\partial \delta_j^{v\alpha}} + \frac{\partial \psi^\alpha}{\partial \dot{\delta}_j^{v\alpha}} \right) \dot{\delta}_j^{v\alpha} - \left( \frac{\partial W^\alpha}{\partial \delta_j^{p\alpha}} + \frac{\partial \psi^\alpha}{\partial \dot{\delta}_j^{p\alpha}} \right) \dot{\delta}_j^{p\alpha} \\ & - \left( \frac{\partial W^\alpha}{\partial D_j^\alpha} + \frac{\partial \psi^\alpha}{\partial \dot{D}_j^\alpha} \right) \dot{D}_j^\alpha - \left( \frac{\partial W^\alpha}{\partial \theta_j^\alpha} + \varphi^\alpha S^\alpha \right) \dot{\theta}_j^\alpha - \left( \varphi^\alpha \frac{\theta_{,j}^\alpha}{\theta} + \frac{\partial \psi^\alpha}{\partial q_j^\alpha} \right) q_j^\alpha = 0 \end{aligned} \quad (21)$$

which yields a set of following relations that are similar to Eqs. 14a–14f, but apply to inter-granular interactions:

$$f_j^\alpha = \frac{\partial W^\alpha}{\partial \delta_j^\alpha} \quad (22a)$$

$$\frac{\partial W^\alpha}{\partial \delta_j^{p\alpha}} + \frac{\partial \psi^\alpha}{\partial \delta_j^{p\alpha}} = 0 \quad (22b)$$

$$\frac{\partial W^\alpha}{\partial D_j^\alpha} + \frac{\partial \psi^\alpha}{\partial \dot{D}_j^\alpha} = 0 \quad (22c)$$

$$\frac{\partial W^\alpha}{\partial \delta_j^{v\alpha}} + \frac{\partial \psi^\alpha}{\partial \dot{\delta}_j^{v\alpha}} = 0 \quad (22d)$$

$$S^\alpha = -\frac{1}{\varphi^\alpha} \frac{\partial W^\alpha}{\partial \theta_j^\alpha} \quad (22e)$$

$$\theta_{,j}^\alpha = -\frac{\theta}{\varphi^\alpha} \frac{\partial \psi^\alpha}{\partial q_j^\alpha} \quad (22f)$$

Equation 22a defines the micro-scale quasi-conservative inter-granular force,  $f_j^\alpha$ , Eqs. 22b through 22c serve as the micro-scale orthogonality conditions, Eq. 22e gives the expression for the micro-scale entropy production, and Eq. 22f gives the temperature gradient between two grains at the  $\alpha$ -th contact. For further discussion, we focus upon Eqs. 16, 17a–17c, and 22a–22d, and discard the temperature effects. We note, however, that Eqs. 17d–17e and 22e–22f are relevant to analysis of thermodynamic temperature and thermal conduction which will be pursued separately.

#### 2.4 Rate-dependent inter-granular damage relationships

For further discussion, we make particular choices for inter-granular interactions to illustrate the applicability of the relationships derived in Sect. 2.2 to rate-dependent granular solids with damage and plasticity. To this end, we consider the inter-granular displacement,  $\delta_j^\alpha$ , to be decomposed into a part purely elastic and a part that is rate-dependent

$$\delta_j^\alpha = \delta_j^{e\alpha} + \delta_j^{v\alpha} \quad (23)$$

The free energy and dissipative potential at the micro-scale for a rate-dependent material with damage and plasticity can be conveniently written as follows in terms of the normal and shear components following the kinematic decomposition described in Sect. 2.1

$$\begin{aligned} W^\alpha &= W_n^\alpha + W_w^\alpha \\ \psi^\alpha &= \psi_n^\alpha + \psi_w^\alpha \end{aligned} \quad (24)$$

The choice of above additive decomposition of inter-granular free energy and dissipative potential is one of simplicity. Alternative formulations of these inter-granular quantities can be conceived that incorporate normal and shear coupling terms to further enrich the inter-granular behavior. For example, coupled normal and shear dissipation is a widely discussed feature of frictional granular materials. The inter-granular free energy are assumed to take the following quadratic form (part associated with the purely elastic deformation and part associated with the rate-dependent process that undergoes damage and plasticity)

$$\begin{aligned} W_n^\alpha &= \frac{1}{2} E_1^\alpha (\delta_n^{e\alpha})^2 + \frac{1}{2} E_n^\alpha (1 - D_n^\alpha) (\delta_n^{v\alpha})^2 (1 - \beta_n^\alpha) \\ W_w^\alpha &= \frac{1}{2} G_1^\alpha (\delta_w^{e\alpha})^2 + \frac{1}{2} G_w^\alpha (1 - D_w^\alpha) (\delta_w^{v\alpha})^2 (1 - \beta_w^\alpha) \end{aligned} \quad (25)$$

where  $E_1$ ,  $E_n$ ,  $G_1$ , and  $G_w$  denote inter-granular stiffnesses, and  $D_n$  and  $D_w$  denote inter-granular damage in the normal and shear directions, respectively. Further,  $\beta_n^\alpha$  and  $\beta_w^\alpha$  are constant non-dimensional plastic

parameters that define the plastic displacements as a proportion of the inter-granular displacements,  $\delta_n^{v\alpha}$  and  $\delta_w^{v\alpha}$ , associated with the viscous element,

$$\beta_n^\alpha = \frac{\delta_n^{p\alpha}}{\delta_n^{v\alpha}}; \quad \beta_w^\alpha = \frac{\delta_w^{p\alpha}}{\delta_w^{v\alpha}} \quad (26)$$

where  $\delta_n^{p\alpha}$  and  $\delta_w^{p\alpha}$  are the inter-granular plastic displacements in normal and shear directions, respectively. We note the plastic parameters  $\beta_n^\alpha$  and  $\beta_w^\alpha$  take a value between 0 and 1, where a value of zero implies an absence of plastic dissipation. On the other hand, a value of 1 will lead to the second term in Eq. 25 or the rate-dependent process making no contribution to the free energy. Combining Eqs. 25 and 26, inter-granular free energy takes the following form:

$$\begin{aligned} W_n^\alpha &= \frac{1}{2} E_1^\alpha (\delta_n^{e\alpha})^2 + \frac{1}{2} E_n^\alpha (1 - D_n^\alpha) \delta_n^{v\alpha} (\delta_n^{v\alpha} - \delta_n^{p\alpha}) \\ W_w^\alpha &= \frac{1}{2} G_1^\alpha (\delta_w^{e\alpha})^2 + \frac{1}{2} G_w^\alpha (1 - D_w^\alpha) \delta_w^{v\alpha} (\delta_w^{v\alpha} - \delta_w^{p\alpha}) \end{aligned} \quad (27)$$

The inter-granular dissipation potential are taken as the sum of the viscous, damage and plastic dissipation in the following classical form [59]

$$\begin{aligned} \psi_n^\alpha &= \frac{1}{2} \mu_n^\alpha (\dot{\delta}_n^{v\alpha})^2 + Y_n^\alpha |\dot{D}_n^\alpha| + Z_n^\alpha |\dot{\delta}_n^{v\alpha}| \\ \psi_w^\alpha &= \frac{1}{2} \mu_w^\alpha (\dot{\delta}_w^{v\alpha})^2 + Y_w^\alpha |\dot{D}_w^\alpha| + Z_w^\alpha |\dot{\delta}_w^{v\alpha}| \end{aligned} \quad (28)$$

where  $\mu_n$  and  $\mu_w$  denote inter-granular viscosities, and the terms  $Y$  and  $Z$  denote generalized forces that are conjugates of the inter-granular damage and plastic dissipation, respectively. In light of Eq. 26, it is useful to rewrite Eq. 28 by splitting the plastic dissipation potential as follows:

$$\begin{aligned} \psi_n^\alpha &= \frac{1}{2} \mu_n^\alpha (\dot{\delta}_n^{v\alpha})^2 + Y_n^\alpha |\dot{D}_n^\alpha| + Z_{1n}^\alpha |\dot{\delta}_n^{v\alpha}| + Z_{2n}^\alpha |\dot{\delta}_n^{p\alpha}| \\ \psi_w^\alpha &= \frac{1}{2} \mu_w^\alpha (\dot{\delta}_w^{v\alpha})^2 + Y_w^\alpha |\dot{D}_w^\alpha| + Z_{1w}^\alpha |\dot{\delta}_w^{v\alpha}| + Z_{2w}^\alpha |\dot{\delta}_w^{p\alpha}| \end{aligned} \quad (29)$$

The grain scale free energy and dissipation defined in Eqs. 25–29 represent a coupled damage and plasticity wherein the dissipation due to damage is partly independent and partly coupled with plasticity. Similar coupling has been proposed in the context of purely continuum modeling (see among others [60–63]). We now apply the grain scale orthogonality condition given in Eq. 22b along with Eqs. 27 and 29 to obtain the ‘dissipative force’ dual of inter-granular plastic displacements  $\delta_n^{p\alpha}$  and  $\delta_w^{p\alpha}$  denoted by  $\chi_n^{p\alpha}$  and  $\chi_w^{p\alpha}$  as follows:

$$\chi_n^\alpha = -\frac{\partial W^\alpha}{\partial \delta_n^{p\alpha}} = Z_{2n}^\alpha \text{sign}(\dot{\delta}_n^{p\alpha}); \quad \chi_w^\alpha = -\frac{\partial W^\alpha}{\partial \delta_w^{p\alpha}} = Z_{2w}^\alpha \text{sign}(\dot{\delta}_w^{p\alpha}) \quad (30a)$$

where

$$Z_{2n}^\alpha = \frac{1}{2} E_n^\alpha (1 - D_n) \delta_n^{v\alpha}; \quad Z_{2w}^\alpha = \frac{1}{2} G_w^\alpha (1 - D_w) \delta_w^{v\alpha} \quad (30b)$$

It is clear from Eq. 30a that the ‘dissipative force’  $\chi_n^{p\alpha}$  and  $\chi_w^{p\alpha}$  should take the same sign as the rate of inter-granular plastic displacements, which implies that plastic displacement should vanish during unloading and that during loading,  $Z_{2n}^{p\alpha} = \chi_n^{p\alpha}$  and  $Z_{2w}^{p\alpha} = \chi_w^{p\alpha}$ . It is a matter of straightforward algebra to show that

$$Z_{1n}^\alpha = \frac{1}{2} E_n (1 - D_n) \delta_n^{p\alpha}; \quad Z_{1w}^\alpha = \frac{1}{2} G_w (1 - D_w) \delta_w^{v\alpha} \quad (31)$$

such that the dissipation potential in Eq. 29 reduces to that of the classical form given in Eq. 28, where

$$Z_n^\alpha = \beta_n^\alpha E_n (1 - D_n) \delta_n^{v\alpha}; \quad Z_w^\alpha = \beta_w^\alpha G_w (1 - D_w) \delta_w^{v\alpha} \quad (32)$$

Further, the application of the micro-scale orthogonality condition given in Eq. 22c, in combination with Eqs. 27 and 29, yields the micro-scale generalized force,  $Y$ , the dual of inter-granular damage  $D$  as follows

$$Y_n^\alpha = \frac{1}{2} E_n^\alpha (\delta_n^{v\alpha})^2 (1 - \beta_n^\alpha); \quad Y_w^\alpha = \frac{1}{2} G_w^\alpha (\delta_w^{v\alpha})^2 (1 - \beta_w^\alpha) \quad (33)$$

These expressions show that the generalized force is the undamaged elastic energy associated with the rate-dependent inter-granular process. Note that, the terms that cross-link normal and shear components do not appear in this particular inter-granular interaction, and the response on the shear plane ( $s$ - $t$  plane) is taken to be isotropic. We find it noteworthy to comment that in the granular systems composed of many components, possibilities of sinks that trap the macroscopic energy in microscopic (grain scale) motions may be present as shown by [64–66]. Further in lattice models, dissipation due to rupture of elastic links are used for describing material damage [67–69]. Such losses are modeled in the approach presented here in a phenomenological sense using contact dissipation mechanism given by Eq. 29.

Now using Eqs. 22a and 23–25, the inter-granular forces are obtained as follows

$$\begin{aligned} f_n^\alpha &= \frac{\partial W^\alpha}{\partial \delta_n^\alpha} = E_1^\alpha (\delta_n^\alpha - \delta_n^{v\alpha}) \\ f_w^\alpha &= \frac{\partial W^\alpha}{\partial \delta_w^\alpha} = G_1^\alpha (\delta_w^\alpha - \delta_w^{v\alpha}) \end{aligned} \quad (34)$$

Finally, using the grain scale orthogonality condition in Eq. 22d, we can find the grain scale constitutive relationships during loading as follows:

$$\begin{aligned} -E_1^\alpha (\delta_n^\alpha - \delta_n^{v\alpha}) + E_n^\alpha \delta_n^{v\alpha} (1 - D_n^\alpha) - \frac{1}{2} E_n^\alpha \delta_n^{p\alpha} (1 - D_n^\alpha) + \mu_n^\alpha \dot{\delta}_n^{v\alpha} + Z_{1n}^\alpha &= 0 \\ -G_1^\alpha (\delta_w^\alpha - \delta_w^{v\alpha}) + G_w^\alpha \delta_w^{v\alpha} (1 - D_w^\alpha) - \frac{1}{2} G_w^\alpha \delta_w^{p\alpha} (1 - D_w^\alpha) + \mu_w^\alpha \dot{\delta}_w^{v\alpha} + Z_{1w}^\alpha &= 0 \end{aligned} \quad (35)$$

Combining Eqs. 31, 34 and 35, the inter-granular constitutive relationships are simplified as follows

$$\begin{aligned} f_n^\alpha &= K_n^\alpha \delta_n^\alpha + \eta_n^\alpha \dot{\delta}_n^\alpha - \zeta_n^\alpha \dot{f}_n^\alpha \\ f_w^\alpha &= K_w^\alpha \delta_w^\alpha + \eta_w^\alpha \dot{\delta}_w^\alpha - \zeta_w^\alpha \dot{f}_w^\alpha \end{aligned} \quad (36)$$

where  $K$ ,  $\eta$  and  $\zeta$  can be interpreted as the inter-granular stiffness, viscosity and relaxation parameters, respectively given as

$$\begin{aligned} K_n^\alpha &= \frac{E_1^\alpha E_n^\alpha (1 - D_n^\alpha)}{E_1^\alpha + E_n^\alpha (1 - D_n^\alpha)}; \quad \eta_n^\alpha = \frac{E_1^\alpha \mu_n^\alpha}{E_1^\alpha + E_n^\alpha (1 - D_n^\alpha)}; \quad \zeta_n^\alpha = \frac{\mu_n^\alpha}{E_1^\alpha + E_n^\alpha (1 - D_n^\alpha)}; \\ K_w^\alpha &= \frac{G_1^\alpha G_w^\alpha (1 - D_w^\alpha)}{G_1^\alpha + G_w^\alpha (1 - D_w^\alpha)}; \quad \eta_w^\alpha = \frac{G_1^\alpha \mu_w^\alpha}{G_1^\alpha + G_w^\alpha (1 - D_w^\alpha)}; \quad \zeta_w^\alpha = \frac{\mu_w^\alpha}{G_1^\alpha + G_w^\alpha (1 - D_w^\alpha)} \end{aligned} \quad (37)$$

Equation 36 can also be written in an alternate form

$$\begin{aligned} f_n^\alpha &= K_n^\alpha (\delta_n^\alpha - \delta_n^{p\alpha}) + \tau_{n\delta}^\alpha K_n^\alpha \dot{\delta}_n^\alpha - \tau_{nf}^\alpha \dot{f}_n^\alpha \\ f_w^\alpha &= K_w^\alpha (\delta_w^\alpha - \delta_w^{p\alpha}) + \tau_{w\delta}^\alpha K_w^\alpha \dot{\delta}_w^\alpha - \tau_{wf}^\alpha \dot{f}_w^\alpha \end{aligned} \quad (38)$$

where  $\tau_{n\delta}$  and  $\tau_{w\delta}$  are the retardation times, and  $\tau_{nf}$  and  $\tau_{wf}$  is the relaxation times given as follows:

$$\begin{aligned} \tau_{n\delta}^\alpha &= \frac{\mu_n^\alpha}{E_n^\alpha (1 - D_n^\alpha)}; \quad \tau_{nf}^\alpha = \frac{\mu_n^\alpha}{E_1^\alpha + E_n^\alpha (1 - D_n^\alpha)}; \\ \tau_{w\delta}^\alpha &= \frac{\mu_w^\alpha}{G_n^\alpha (1 - D_w^\alpha)}; \quad \tau_{wf}^\alpha = \frac{\mu_w^\alpha}{G_1^\alpha + G_n^\alpha (1 - D_w^\alpha)} \end{aligned} \quad (39)$$

It is clear from Eqs. 36–39 that the assumed form of inter-granular free energy and dissipation potential leads to a three-parameter nonlinear inter-granular constitutive law of Zener solid type. Other types of micro-scale

laws can be introduced that are valid for materials such as granular soils [31] and polyurea [70]. Furthermore, the micro-scale laws derived here can serve for modeling rate-dependent damage and plasticity of octet-truss lattices discussed in [71].

To complete the inter-granular constitutive relationships for coupled damage-plasticity, we introduce the following criterion for unloading and reloading, utilizing inter-granular yield criterion  $F_n^\alpha$  and  $F_w^\alpha$ , defined independently for the normal and shear directions as:

$$F_n^\alpha = F_n^\alpha (\delta_n^{v\alpha}, \delta_n^{p\alpha}, D_n^\alpha) = 0; \quad \text{and} \quad F_w^\alpha = F_w^\alpha (\delta_w^{v\alpha}, \delta_w^{p\alpha}, D_w^\alpha) = 0 \quad (40)$$

The loading, unloading and reloading conditions at the inter-granular scale can now be described as follows:

- (1) Loading— $F_n^\alpha = 0$ , and  $\dot{\delta}_n^{v\alpha} > 0$ , and  $F_w^\alpha = 0$ , and  $\dot{\delta}_w^{v\alpha} > 0$ .
- (2) Unloading— $F_n^\alpha < 0$ , and  $\dot{\delta}_n^{v\alpha} < 0$ , and  $F_w^\alpha < 0$ , and  $\dot{\delta}_w^{v\alpha} < 0$ .
- (3) Reloading— $F_n^\alpha < 0$ , and  $\dot{\delta}_n^{v\alpha} > 0$ , and  $F_w^\alpha < 0$ , and  $\dot{\delta}_w^{v\alpha} > 0$ .

In this case, the inter-granular flow rule can also be defined to obtain the inter-granular ‘dissipative forces’  $\chi_n^{p\alpha}$  and  $\chi_w^{p\alpha}$  as follows

$$\chi_n^{p\alpha} = \lambda_n^{p\alpha} \frac{\partial F_n^\alpha}{\partial \delta_n^{p\alpha}}; \quad \chi_w^{p\alpha} = \lambda_w^{p\alpha} \frac{\partial F_w^\alpha}{\partial \delta_w^{p\alpha}} \quad (41)$$

where  $\lambda_n^\alpha$  and  $\lambda_w^\alpha$  are plastic multipliers. The yield criteria can be obtained from the plastic dissipation defined previously which gives

$$\begin{aligned} F_n^\alpha &= \frac{1}{2} E_n^\alpha \beta_n^\alpha \left[ (1 - D_n^\alpha) (\delta_n^{v\alpha})^2 - (1 - \max D_n^\alpha) (\max \delta_n^{v\alpha})^2 \right] = 0; \\ F_w^\alpha &= \frac{1}{2} G_w^\alpha \beta_w^\alpha \left[ (1 - D_w^\alpha) (\delta_w^{v\alpha})^2 - (1 - \max D_w^\alpha) (\max \delta_w^{v\alpha})^2 \right] = 0 \end{aligned} \quad (42)$$

where the left superscript ‘max’ denoted the maximum accumulated values of the corresponding quantities. We can see that introducing Eqs. 42 and 26 into 41, we will find the ‘dissipative forces’  $\chi_n^{p\alpha}$  and  $\chi_w^{p\alpha}$  to be same as obtained in Eq. 30. During unloading and reloading, the dissipation vanishes; therefore, the multipliers  $\lambda_n^\alpha$  and  $\lambda_w^\alpha$  takes a value of zero, while they take a value 1 during loading. As usual, the plastic potential  $F_n^\alpha$  and  $F_w^\alpha$  satisfy the Karush–Kuhn–Tucker (KKT) type conditions of complementarity and consistency stated as

$$\begin{aligned} F_n^\alpha \lambda_n^\alpha &= 0 \quad \text{and} \quad \dot{F}_n^\alpha \lambda_n^\alpha = 0 \\ F_w^\alpha \lambda_w^\alpha &= 0 \quad \text{and} \quad \dot{F}_w^\alpha \lambda_w^\alpha = 0 \end{aligned} \quad (43)$$

Further, the grain scale constitutive relationships during unloading process can be derived as follows:

$$\begin{aligned} f_n^\alpha &= K_n^{u\alpha} (\delta_n^\alpha - \beta_n^{\alpha \max} \delta_n^{v\alpha}) + \eta_n^{u\alpha} \dot{\delta}_n^\alpha - \zeta_n^{u\alpha} \dot{f}_n^\alpha \\ f_w^\alpha &= K_w^{u\alpha} (\delta_w^\alpha - \beta_w^{\alpha \max} \delta_w^{v\alpha}) + \eta_w^{u\alpha} \dot{\delta}_w^\alpha - \zeta_w^{u\alpha} \dot{f}_w^\alpha \end{aligned} \quad (44)$$

where  $K^u$ ,  $\eta^u$  and  $\zeta^u$  are the unloading inter-granular stiffness, viscosity and relaxation parameters, respectively, given as

$$\begin{aligned} K_n^{u\alpha} &= \frac{E_1^\alpha E_n^{u\alpha}}{E_1^\alpha + E_n^{u\alpha}}; \quad \eta_n^{u\alpha} = \frac{E_1^\alpha \mu_n^\alpha}{E_1^\alpha + E_n^{u\alpha}}; \quad \zeta_n^{u\alpha} = \frac{\mu_n^\alpha}{E_1^\alpha + E_n^{u\alpha}}; \\ K_w^{u\alpha} &= \frac{G_1^\alpha G_w^{u\alpha}}{G_1^\alpha + G_w^{u\alpha}}; \quad \eta_w^{u\alpha} = \frac{G_1^\alpha \mu_w^\alpha}{G_1^\alpha + G_w^{u\alpha}}; \quad \zeta_w^{u\alpha} = \frac{\mu_w^\alpha}{G_1^\alpha + G_w^{u\alpha}} \end{aligned} \quad (45)$$

here,  $E_n^{u\alpha} = \frac{E_n^\alpha (1 - \max D_n^\alpha)}{(1 - \beta_n^\alpha)}$ ; and  $G_w^{u\alpha} = \frac{G_w^\alpha (1 - \max D_w^\alpha)}{(1 - \beta_w^\alpha)}$ .

## 2.5 Constitutive relationship for granular systems

The constitutive relationship for an VE of a granular system can now be obtained by introducing Eq. 36 or 44 into Eq. 16. However, there are practical difficulties associated with relating inter-granular relative displacements and the VE strain. To resolve this difficulty, we consider Eq. 16 in light of Eq. 3, which gives

$$\sigma_{ij} = \frac{1}{V} \sum_{\alpha=1}^N f_k^\alpha l_l^\alpha \frac{\partial \varepsilon_{kl}^n}{\partial \varepsilon_{ij}} \quad \text{where } \varepsilon_{kl}^n = u_{(k,l)}^n \quad (46a)$$

and adopt as a first approximation a mean field kinematical assumption [18,34] for relating the grain scale displacement gradient to the overall VE displacement gradient such that

$$\varepsilon_{kl}^n = \varepsilon_{ij}; \quad \frac{\partial \varepsilon_{kl}^n}{\partial \varepsilon_{ij}} = \delta_{ik} \delta_{jl}; \quad \text{and} \quad \delta_k^\alpha = \varepsilon_{kl} l_l^\alpha \quad (46b)$$

in which strain  $\varepsilon_{kl}$  is the symmetric part of the displacement gradient. We note that the relationship between the grain scale displacement gradient and the overall VE displacement gradient is, in general, complex for random granular materials as discussed in [34]. In principle, it is possible to relate the grain scale displacement gradient to the overall displacement gradient using a fluctuation terms or shift vectors, which have to be determined though energy minimization or by enforcing grain scale equilibrium provided the complete microstructure is known [34]. In the case of disordered systems, such analysis is tantamount to obtaining solution of the particle displacement field within a simulated granular structure at large computational cost. For materials with ill-defined random structure, wide-ranging, often unrealistic assumptions are made to simulate some ‘reasonable’ granular microstructure or some meso-scale (intermediate scale) structure introduced comprising particle clusters. These simulated structures have to be analyzed using discrete methods or other homogenization schemes to determine the fluctuation terms as discussed in our earlier work [30,34]. In contrast, the mean field kinematical assumption (or a mean field statical assumption), albeit approximate, provides a feasible approach for the derivation of the VE constitutive law and has been shown to describe a number of phenomena exhibited by granular materials for judiciously chosen inter-granular force laws [10,31,35,72]. Therefore, in this paper, we use the mean field assumption of Eq. 46b, and compute the average stress tensor of an VE as:

$$\sigma_{ij} = \frac{1}{V} \sum_{\alpha=1}^N f_i^\alpha l_j^\alpha \quad (47)$$

We observe that Eq. 47 is a widely used expression for Cauchy stress tensor in granular mechanics [58]. Similar expression has been derived using the virial of Clausius [73,74], as well as in the statistical mechanics of fluids [75,76] and has been a subject of recent discussion in the context of molecular and atomistic modeling [77,78]. For sufficiently large VE containing variously oriented inter-granular interactions, the summation in Eq. 47 can be approximated by the following integral under certain simplifying assumptions [10,17,58]

$$\sigma_{ij} = Nl \int_0^{2\pi} \int_0^\pi f_j(\theta, \phi) n_i(\theta, \phi) \xi(\theta, \phi) \sin \theta d\theta d\phi \quad (48)$$

where  $N$  is the number density of pair interactions,  $l$  is the average grain size,  $n_i$  is a unit vector expressed in terms of the spherical coordinates  $(\theta, \phi)$  and  $\xi(\theta, \phi)$  is a directional probability density function such that the product  $N\xi(\theta, \phi) \sin \theta d\theta d\phi$  gives the number density of pair interactions in the solid angle  $\sin \theta d\theta d\phi$ . For convenience, we incorporate the factor  $Nl$  with the force,  $f_j$ , such that it is expressed as a traction and normalize the relative displacement,  $\delta_i$ , with  $l$ . The units of the stiffness and viscosity in Eqs. 36–37 and 44–45 are appropriately modified. Now, by combining Eqs. 36 or 44 and 48, the following differential form of rate constitutive relationship can be obtained

$$\sigma_{ij} = \int_0^{2\pi} \int_0^\pi (K_{jk} n_l \varepsilon_{kl} + \eta_{jk} n_l \dot{\varepsilon}_{kl} + \zeta_{jk} \dot{f}_k) n_i \xi(\theta, \phi) \sin \theta d\theta d\phi \quad (49)$$

where the inter-granular stiffness, viscosity, and relaxation tensors are given as

$$\begin{aligned} K_{ij}(t) &= K_n(t)n_i n_j + K_w(t)(s_i s_j + t_i t_j) \\ \eta_{ij}(t) &= \eta_n(t)n_i n_j + \eta_w(t)(s_i s_j + t_i t_j) \\ \zeta_{ij}(t) &= \zeta_n(t)n_i n_j + \zeta_w(t)(s_i s_j + t_i t_j) \end{aligned} \quad (50)$$

### 3 Results and discussion

To demonstrate the applicability of the above-derived model, it is numerically evaluated for a particular nonlinear damage and viscous dissipation model. In the subsequent discussion, we present (1) an efficient numerical implementation of the model, (2) the expressions for inter-granular damage and viscosity and (3) a comparison with experimental results for creep, creep-recovery and 3-point bending behavior. We then discuss the advantages this type of model provides by investigating how the inter-granular elastic and dissipative energies as well as damage and plasticity evolve at different stress levels for creep, creep-recovery and monotonic loading.

#### 3.1 Numerical implementation

Since the inter-granular stiffness, viscosity, and relaxation parameters are in general nonlinear functions of force and displacements, a numerical approach is required to evaluate the constitutive relationship in Eq. 49. For developing a numerical procedure, we first consider the time discretization of the inter-granular constitutive relationship in Eq. 36. Using the backward Euler method, we get from Eq. 36a:

$$f_n^t = K_n^t \delta_n^t + \eta_n^t \frac{(\delta_n^t - \delta_n^{t-\Delta t})}{\Delta t} - \zeta_n^t \frac{(f_n^t - f_n^{t-\Delta t})}{\Delta t} \quad (51)$$

The inter-granular normal force,  $f_n^t$ , at the current time,  $t$ , can then be written in the following form

$$f_n^t = C_n^t \delta_n^t + P_n^t \delta_n^{t-\Delta t} + Q_n^t f_n^{t-\Delta t} \quad (52)$$

where

$$C_n^t = \frac{K_n^t \Delta t + \eta_n^t}{\Delta t + \zeta_n^t}; P_n^t = -\frac{\eta_n^t}{\Delta t + \zeta_n^t}; \text{ and } Q_n^t = \frac{\zeta_n^t}{\Delta t + \zeta_n^t} \quad (53)$$

Equation 26b can be treated in the same manner such that

$$f_w^t = C_w^t \delta_w^t + P_w^t \delta_w^{t-\Delta t} + Q_w^t f_w^{t-\Delta t} \quad (54)$$

where

$$C_w^t = \frac{K_w^t \Delta t + \eta_w^t}{\Delta t + \zeta_w^t}; P_w^t = -\frac{\eta_w^t}{\Delta t + \zeta_w^t}; \text{ and } Q_w^t = \frac{\zeta_w^t}{\Delta t + \zeta_w^t} \quad (55)$$

We note that the coefficients,  $C$ ,  $P$  and  $Q$  in Eqs. 53 and 55 are functions of force,  $f$ , and displacement,  $\delta$ , at time,  $t$ . Equations 52 and 54 are thus nonlinear implicit functions of  $f$  and  $\delta$  and can be expressed in the following general form after dropping, for convenience, the subscripts  $n$ , and  $w$ , superscript  $t$ , and replacing  $t - \Delta t$  with 0

$$R(f, \delta) \equiv f - C(f, \delta) \delta - P(f, \delta) \delta^0 - Q(f, \delta) f^0 = 0 \quad (56)$$

where  $R(f, \delta)$  denotes a residual force.

We now utilize Newton's method and expand the residual,  $R(f, \delta)$ , in Taylor series as follows

$$R(f, \delta) = R(i^{-1} f, i^{-1} \delta) + \left[ \frac{\partial R}{\partial \delta} \right]^{i-1} \Delta \delta + \left[ \frac{\partial R}{\partial f} \right]^{i-1} \Delta f \quad (57)$$

where the right superscript,  $i - 1$ , refers to the iteration step and the terms of order 2 or higher have been omitted. Combining Eqs. 56 and 57, we get

$$\left(1 - {}^{i-1}R_f\right) \Delta f = \left({}^{i-1}C + {}^{i-1}R_\delta\right) \Delta\delta + {}^{i-1}C {}^{i-1}\delta + {}^{i-1}P\delta^0 + {}^{i-1}Qf^0 - {}^{i-1}f \quad (58)$$

where

$${}^{i-1}R_\delta = {}^{i-1}\left(\frac{\partial C}{\partial\delta}\delta + \frac{\partial P}{\partial\delta}\delta^0 + \frac{\partial Q}{\partial\delta}f^0\right); \quad \text{and} \quad {}^{i-1}R_f = {}^{i-1}\left(\frac{\partial C}{\partial f}\delta + \frac{\partial P}{\partial f}\delta^0 + \frac{\partial Q}{\partial f}f^0\right) \quad (59)$$

and the force and displacements at the  $i$ -th iteration are updated in the usual manner as

$${}^i f = {}^{i-1} f + \Delta f \quad \text{and} \quad {}^i \delta = {}^{i-1} \delta + \Delta\delta \quad (60)$$

The above iterative scheme can be computationally intense, especially from the point of view of implementation into numerical schemes for initial boundary value problems (IBVP); therefore, an explicit scheme is desirable. To this end, we observe from Eq. 58 that  ${}^{i-1}R_f\Delta f$  and  ${}^{i-1}R_\delta\Delta\delta$  contain product terms as well as terms proportional to  $\Delta t^2$ , which, for sufficiently small loading increments and  $\Delta t$ , can be negligibly small compared to the remaining terms. In this case Eq. 58 is simplified and the coefficients  $C$ ,  $P$  and  $Q$  are evaluated at previous time step  $t = t - \Delta t$  after ignoring the subsequent iterations:

$$f^t = f^{t-\Delta t} + \Delta f = C^{t-\Delta t} \left(\delta^{t-\Delta t} + \Delta\delta\right) + P^{t-\Delta t} \delta^{t-\Delta t} + Q^{t-\Delta t} f^{t-\Delta t} \quad (61)$$

We note that the numerical scheme may be further refined especially near failure points using the technique presented in [79,80], which provide a method for finding solution with large loading step. Substituting the inter-granular force from Eq. 61 into Eq. 49, we get an explicit form of the stress-strain relationship at time  $t$

$$\sigma_{ij}^t = C_{ijkl}^{t-\Delta t} \varepsilon_{kl}^t + P_{ijkl}^{t-\Delta t} \varepsilon_{kl}^{t-\Delta t} + \tilde{\sigma}_{ij}^{t-\Delta t} \quad (62)$$

In Eq. 50, the coefficients are given as

$$C_{ijkl}^{t-\Delta t} = \int_0^{2\pi} \int_0^\pi \left(C_n^{t-\Delta t} n_j n_k + C_w^{t-\Delta t} (t_j t_k + s_j s_k)\right) n_i n_l \xi(\theta, \phi) \sin(\theta) d\theta d\phi \quad (63a)$$

$$P_{ijkl}^{t-\Delta t} = \int_0^{2\pi} \int_0^\pi \left(P_n^{t-\Delta t} n_j n_k + P_w^{t-\Delta t} (t_j t_k + s_j s_k)\right) n_i n_l \xi(\theta, \phi) \sin(\theta) d\theta d\phi \quad (63b)$$

$$\tilde{\sigma}_{ij}^{t-\Delta t} = \int_0^{2\pi} \int_0^\pi \left(Q_n^{t-\Delta t} f_n^{t-\Delta t} n_j + Q_w^{t-\Delta t} f_w^{t-\Delta t} (t_j + s_j)\right) n_i \xi(\theta, \phi) \sin(\theta) d\theta d\phi \quad (63c)$$

The time discretized form of constitutive relationship in Eq. 62 can be efficiently solved by specifying stress, strains or their combinations in an incremental manner. The accuracy and efficiency of the derived numerical procedure has been discussed in [81]. The relationships can be readily implemented into finite element schemes for IBVP or into beam theory as demonstrated later in Sect. 3.4.

### 3.2 Inter-granular damage and viscosity

Damage at the inter-granular scale is modeled by an exponential law [10,35] given by:

$$D_n = 1 - e^{-\left|\frac{\left(\delta_n(t) - \frac{f_n(t)}{E_1}\right)}{B_n}\right|}; \quad \text{and} \quad D_w = 1 - e^{-\left|\frac{\left(\delta_w(t) - \frac{f_w(t)}{G_1}\right)}{B_w}\right|} \quad (64)$$

The viscosities,  $\mu_n$  and  $\mu_w$ , are given by taking into account the damage of the inter-granular interactions as

$$\mu_n(t) = \mu_{n0} e^{-\left| \frac{(\delta_n(t) - \frac{f_n(t)}{E_1})}{\beta B_n} \right|}; \quad \text{and} \quad \mu_w(t) = \mu_{w0} e^{-\left| \frac{(\delta_w(t) - \frac{f_w(t)}{G_1})}{\beta B_w} \right|} \quad (65)$$

To model the asymmetric inter-granular behavior under tensile and compressive actions, we replace the parameters  $B_n$  and  $B_w$  in Eqs. 64 and 65 by  $\alpha_n B_n$  and  $\alpha_w B_w$  for the tensile case, where  $0 \leq \alpha_n < 1$  and  $0 \leq \alpha_w < 1$ . We observe from Eqs. 37 and 64 that model parameters  $E_1$ ,  $E_n$ ,  $\mu_{n0}$  and  $B_n$  describe the elasticity, viscosity and damage behavior of the inter-granular interactions in the normal direction. Similarly, parameters  $G_1$ ,  $G_w$ ,  $\mu_{w0}$ , and  $B_w$  describe the inter-granular interactions in the shear direction. We note here that the parameters  $B_n$  and  $B_w$  govern the displacement at which softening commences at the inter-granular scales. In addition, parameter  $\beta$  determines the displacement at which the viscous element begins to lose integrity. Consequently, these parameters also govern the peak inter-granular forces. From Eqs. 37, 64 and 65, we observe that the inter-granular behavior for  $B_n = B_w = \infty$  and  $B_n = B_w = 0$  is bounded between a Zener solid and a Maxwell material.

### 3.3 Experimental verification and model predictions

The derived model is verified by comparing model predictions with experimental behavior for hot-mix asphalt (HMA) concrete under uniaxial unconfined creep and creep-recovery behavior under compression and tension at a constant temperature of 20°C [3]. We also utilize the model to simulate behavior under monotonic unconfined uniaxial loading at the strain rates of 0.001/s and 0.0005/s. The creep-recovery and monotonic predictions are further elucidated by investigating the calculated elastic and dissipated energies. Finally, the model is applied to simulate 3-point bending experiments on dentin-adhesive polymers.

#### 3.3.1 Calibration and identification of model parameters

The model is calibrated using the experimental creep and creep-recovery data under compressive uniaxial stress  $\sigma_{11} = 1.0$  MPa ( $\sigma_{22} = \sigma_{33} = 0$ ) and tensile creep data at stress  $\sigma_{11} = 0.3$  MPa ( $\sigma_{22} = \sigma_{33} = 0$ ). First, the normal and shear stiffness and viscosity parameters  $E_1$ ,  $G_1$ ,  $G_w$ ,  $E_n$ ,  $\mu_n$  and  $\mu_w$ , were obtained by assuming  $B_n = B_w = \beta = \infty$  and fitting the reduced equation to the initial portion of the experimental creep curve. Thereafter, damage parameters  $B_n$ ,  $B_w$  and  $\beta$  were introduced into the model and optimized to match the complete creep–response curve. Further, normal and shear plastic parameters  $\beta_n$  and  $\beta_w$  were identified to match the creep–recovery curve at 1.0 MPa in compression for a load time of 40 s. We recall that plastic parameters  $0 \leq \beta_n \leq 1$  and  $0 \leq \beta_w \leq 1$ . To account for the asymmetric inter-granular behavior under tension and compression, parameter  $\alpha_n$  and  $\alpha_w$  were included in the model and identified using the tensile creep data at 0.3 MPa stress amplitude. The following model parameters were found:  $G_1 = 0.8E_1$ ,  $G_w = E_n$ ,  $\mu_n = \mu_w$ , and  $B_n = B_w = 14.3 \times 10^{-3}$ ,  $\beta_n = \beta_w$  and  $\alpha_n = \alpha_w$  where,  $E_1 = 2.4$  GPa/m,  $E_n = 0.3$  GPa/m,  $\tau_{n\delta}(0) = 57$  s,  $\tau_{nf}(0) = 6.33$  s and  $\beta = 3.8$ ,  $\beta_n = \beta_w = 0.833$ , and  $\alpha_n = \alpha_w = 0.175$ . The experimental and calibrated creep curves under uniaxial compressive and tensile loads for HMA are shown in Fig. 1. Clearly, the model is able to replicate the primary, secondary and tertiary creep behavior as shown by the close agreement of the calibration and experimental curves at  $\sigma_{11} = 1.0$  MPa and  $\sigma_{11} = 0.3$  MPa for compressive and tensile loads, respectively. Furthermore, after the identification of inter-granular plasticity parameter, model is also able to accurately capture the creep-recovery response shown by HMA under 1.0 MPa compressive stress.

#### 3.3.2 Creep behavior

Figure 2a shows the experimental and calculated creep curves for HMA under uniaxial compressive loading. Clearly, the model is able to replicate the primary, secondary and tertiary creep behavior as shown by the close agreement of the calibration and experimental curves at  $\sigma_{11} = 1.0$  MPa. Furthermore, the model provides a close prediction of the creep behavior at  $\sigma_{11} = 1.5$  MPa and particularly, the creep time-to-failure. To contrast the nonlinear creep behavior, we show, in the inset, the linear viscoelastic response at the two stress levels obtained by ignoring the effects of damage and plasticity. Figure 2b shows the elastic energy density, and the viscous and damage dissipation densities for the two creep tests. We note that in the absence of unloading, plastic dissipation has not been separately calculated and is contained within elastic energy shown in Fig. 2b.

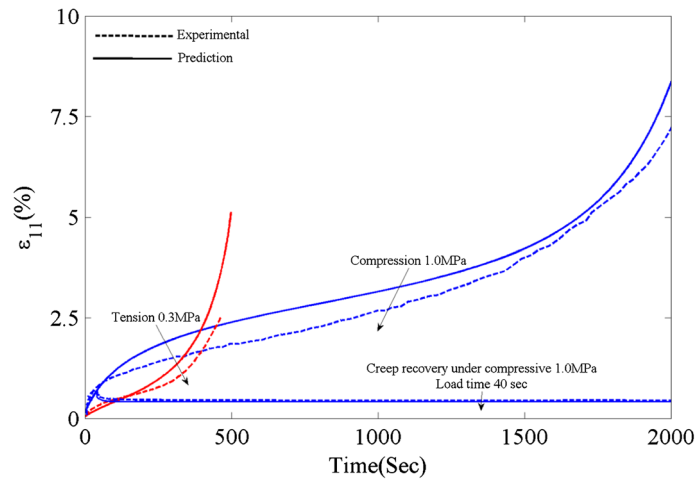


**Fig. 1** Experimental and model predicted creep curves under uniaxial compressive and tensile stress used for model parameter identification

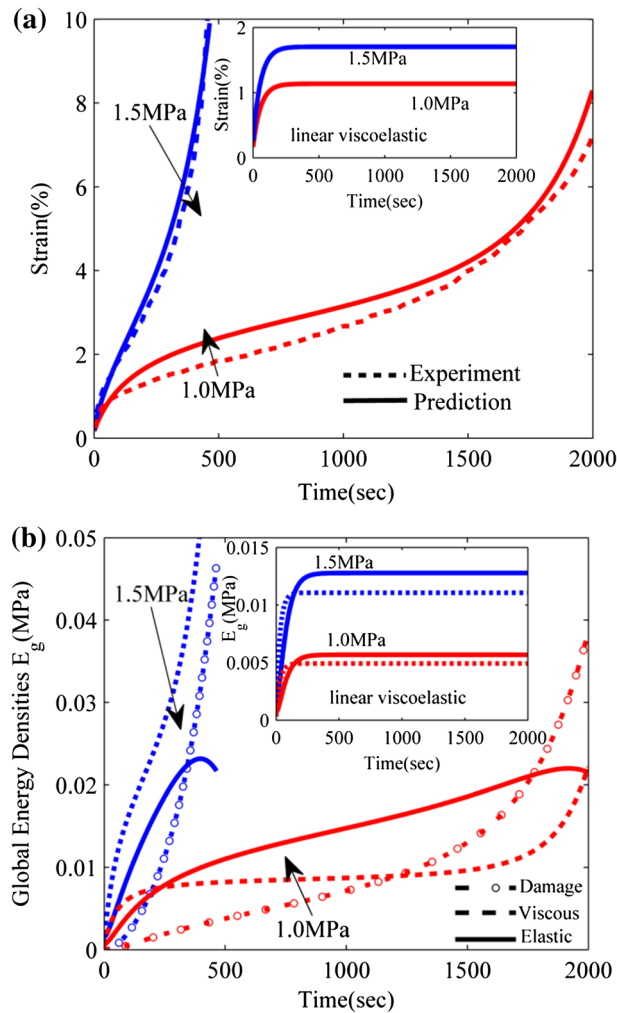


**Fig. 2 a** Experimental and model predicted creep curves for hot mix asphalt at two different stress amplitudes. For contrast, the *inset* shows the linear viscoelastic response obtained by ignoring the effects of damage. **b** Predicted evolution of macro-scale energy densities with time corresponding to the creep curves given of **a**. For contrast, the *inset* shows the evolution of elastic and viscous energies under linear viscoelastic assumption

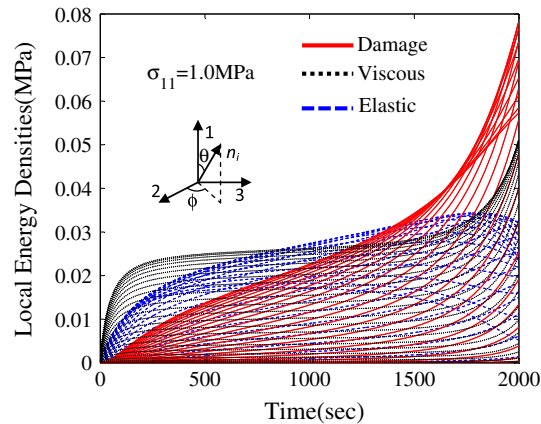


**Fig. 3** Predicted evolution of inter-granular (micro-scale) energy densities with time corresponding to the creep curve for  $\sigma_{11} = 1.0$  MPa

Thus, the elastic energy represents partly the amount of recoverable work at a given time if the applied stress is removed and material is allowed to recover. The inset includes for comparison the elastic energy and viscous dissipation for linear viscoelastic material in which elastic energy will be completely recovered.

We can observe from Fig. 2b that the elastic energy and the viscous dissipation show an initial rapid increase due to the sudden application of load in a creep test. For linear viscoelastic materials, these reach an asymptote beyond a certain characteristic retardation time. In contrast for nonlinear materials with damage, the elastic energy increases at slower rate as secondary creep progresses, reaches a peak during tertiary creep and decreases indicating onset of material failure. The elastic energy can be expected to asymptote to zero if the creep experiment is continued further. The viscous dissipation also slows down during the secondary creep phase, however, shows a rapid increase during tertiary creep and will reach an asymptote at material failure. The damage dissipation, on the other hand, exhibits gradual increase as the material accumulates damage, increasing rapidly during tertiary creep.

During uniaxial creep, damage evolution in the materials is expected to be anisotropic depending upon the loading direction. To illustrate how anisotropic damage develops, it is useful to examine the evolution of inter-granular energy densities and damage. Figure 3 shows the inter-granular energy densities in selected orientations as function of time for creep calculations at  $\sigma_{11} = 1.0$  MPa. Since the loading is axisymmetric, the inter-granular energy densities are independent of azimuthal angle,  $\phi$ . Thus, each curve in Fig. 3 refers to  $\theta$  measured with respect to the loading direction-1 (see inset Fig. 3). From Fig. 3, we can see that the inter-granular elastic energies, and viscous and damage dissipation evolve with time differently in the various directions. For further elucidating the relationship of this evolution with loading direction, polar diagrams are given in Fig. 4 that show the normalized inter-granular energy densities in  $\theta$ -coordinate at selected times. We note that these polar plots are centro-symmetric as well as symmetric about the horizontal plane. The normalization is done with respect to the total energy in a given orientation at any given time, such that the normalized elastic energy, the viscous and the damage dissipation densities, denoted by  $r_e$ ,  $r_v$  and  $r_d$ , respectively, sum to unity ( $r_e + r_v + r_d = 1$ ). Similarly, the evolution of inter-granular damage in the normal and shear directions,  $D_n$  and  $D_w$ , respectively, is plotted as polar diagrams for selected times in Fig. 5.

As the loading commences at time  $t = 0$ , the elastic energy fraction  $r_e$  is unity and viscous and damage energy fractions  $r_v$  and  $r_d$  are both zero. As material undergoes creep deformation, the proportions of elastic energies decrease while that of the viscous and damage dissipation increases, however, in different ratios in the different directions. At  $t = 1$  s, which is a small fraction of the initial inter-granular retardation time of 57 s, the elastic energy and viscous dissipation are in approximately same proportion in all orientations while damage dissipation is negligibly small. As creep deformation progresses, the proportion of damage dissipation increases with maximum in the loading direction. However, in the orientations orthogonal to loading direction, the proportion of elastic energy remains significantly larger till the commencement of tertiary creep at  $t = 1,500$  s. Beyond this time, the proportion of elastic energy begins to reduce while damage dissipation increases in all directions, however, in a characteristically orientation-dependent manner. It is noteworthy that such load-induced anisotropy provides elastic energy densities whose polar plots no longer exhibit a convex shape. These effects can be observed also in simple anisotropic elastic materials belonging to the hexagonal

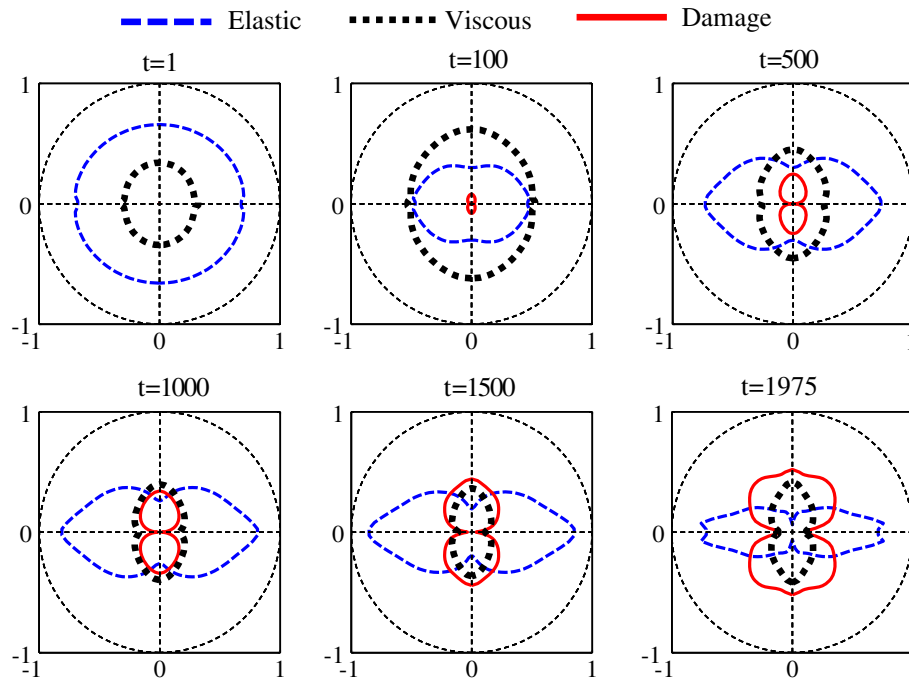


**Fig. 4** Polar plots of inter-granular (micro-scale) energy densities fractions at selected times corresponding to the creep curve for  $\sigma_{11} = 1.0\text{MPa}$

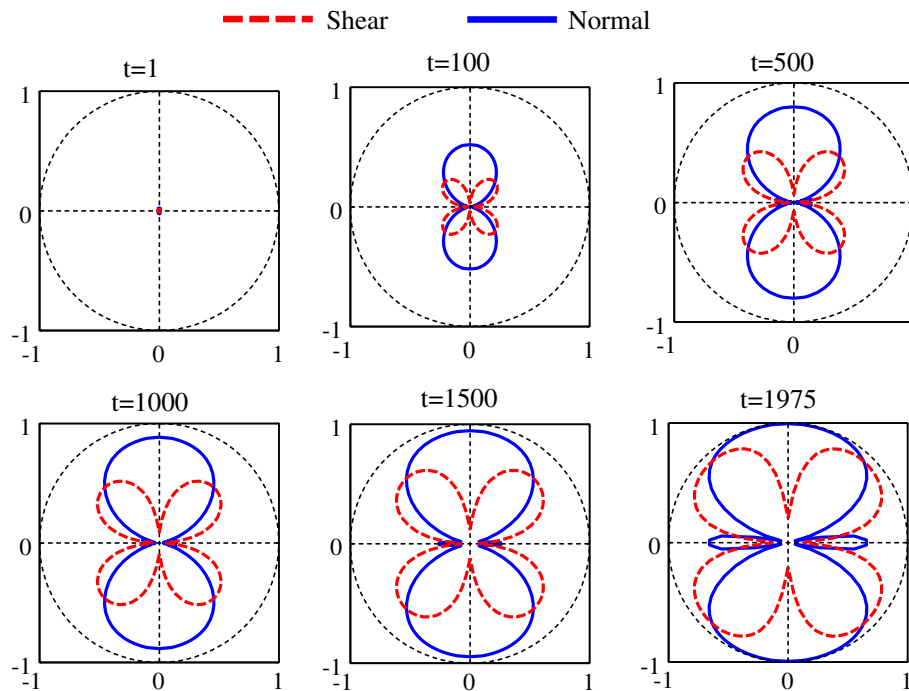


**Fig. 5** Polar plots of inter-granular normal and shear direction damage at selected times corresponding to the creep curve for  $\sigma_{11} = 1.0\text{MPa}$

of tetragonal symmetry classes. Indeed for such anisotropic elastic materials, if we look at the polar plots of Young's modulus as a function of the azimuthal angle  $E = E(\theta)$ —which turns out to be the elastic energy density corresponding to a unit strain—a similar lack of convexity is observed [82, 83]. The anisotropic damage development is seen clearly from the inter-granular damage in normal and shear direction shown in Fig. 5.

These results indicate that the materials undergoing loading–unloading cycles with fixed stress amplitude will progressively develop induced anisotropy. Such effects that manifest due to granular nature of materials are not easily represented by phenomenological constitutive relationships based upon the concepts of traditional Cauchy mechanics or tensorial damage functions.

### 3.3.3 Creep-recovery behavior

Under practical applications, HMA experiences repeated cyclic load imposed by traffic on the roadway. Therefore, it is useful to compare the model prediction with the experimental data under repeated loads. In this work, model predictions are compared with creep-recovery response of HMA under uniaxial compressive and tensile stresses of 1.0 and 0.3 MPa, respectively, under following three different load-unload sequences formed of different load-times (LT) and unload-times (UT), case 1:  $LT = 120$  s,  $UT = 100$  s, case 2:  $LT = 60$  s,  $UT = 100$  s, and case 3:  $LT = 120$  s and  $UT = 1,500$  s.

The predicted and experimental creep curve under uniaxial compressive load of 1.0 MPa at three load sequences is given in Fig. 6. From Fig. 6a, we observe that in case 1 when LT is 120 s and UT is 100 s, model predictions are in close agreement with the experimental data. Not only model predicts both the failure-time and failure-strain correctly but also the amount of plastic or residual strain at the end of each creep-recovery cycle. When the load time is decreased to 60 s in case 2, as expected, HMA samples suffer smaller strain at any given time compared to LT of 120 s as shown in Fig. 6b. The model is able to closely match the creep-recovery response for the first 7 cycles. The model prediction and experimental data diverges beyond 7 cycles with the experimental response showing accelerated creep and sudden failure, whereas model indicates a more gradual increase in creep with a delayed failure. Since the LT is half of that in case 1, the sample undergoes smaller damage and accumulates smaller plastic strain, as the sample is well within its primary creep stage. For case 3 in which when LT is 60 s, but UT is increased to 1,500 s, results are presented in Fig. 6c. In this case, model predictions agree relatively well for the first 11 cycles. Beyond that, the predictions appear to be within the secondary creep regime, that is, the strains during every subsequent creep-recovery cycles increase gradually. The predictions do not show the accelerating trend exhibited by the experimental data. The predicted response is expected since the large UT provides sufficient time for the elastic recovery.

The model capabilities to capture the asymmetric compression–tension behavior is shown in Fig. 7, which gives the comparison of model prediction and experimental data for creep-recovery behavior under 0.30 MPa tensile stress for the three different load–unload sequences. We observe from Fig. 7a that the case 1 model predictions match very closely with the experimental data and predict both the failure-time and strain correctly. For case 2, in which the LT is decreased to 60 s, the model prediction is close for the first 10 cycles. In the subsequent cycles, the model predicts accelerated creep strains reaching failure at a higher strain albeit similar time as that observed in the experiment. For case 3, we observe a much larger discrepancy between the model predictions and the experiments. Although the trends are captured well, the creep strains appear to be larger and recovery much smaller in the experiments than those in the predictions.

With regards to the observed divergence in predicted and experimental data in Figs. 6c and 7c, we note that the material response at such large length of time can be sensitive to small material variability. Therefore, such divergence of close agreement with experimental data can be expected, especially when the parameter identification have been performed with a very small database of results that do not include information on material variability. It is encouraging, nevertheless, that the predicted responses replicate creep-recovery response rather well.

To understand the dissipation behavior during creep-recovery process, we have investigated the elastic energies, and the viscous, damage and plastic dissipation for loading sequence corresponding to Figs. 6a and 7a. Figure 8a, b shows the evolution of the elastic energy, and the viscous, damage and plastic dissipation for the multiple creep-recovery cycles. We observe from Fig. 8 that the damage and plastic energies remain constant during recovery, which is expected since damage and plastic dissipation are assumed to vanish during unloading. During each subsequent creep cycles, the elastic energy becomes proportionally smaller compared do the dissipative energies. As the sample enters a tertiary creep regime accompanied by accelerating creep deformation, the viscous dissipation increases rapidly, although, both damage and plastic dissipation increase as well.

In Fig. 9a, b, we show the creep-recovery curve as well as the evolution of energy densities for the first cycle of creep-recovery loading sequence corresponding to Fig. 6a. We particularly highlight the effect of plasticity on both the creep-recovery and the energy density evolution behavior by considering two scenarios: (1) with only damage and (2) with coupled damage and plasticity. We observed from Fig. 9a that as expected

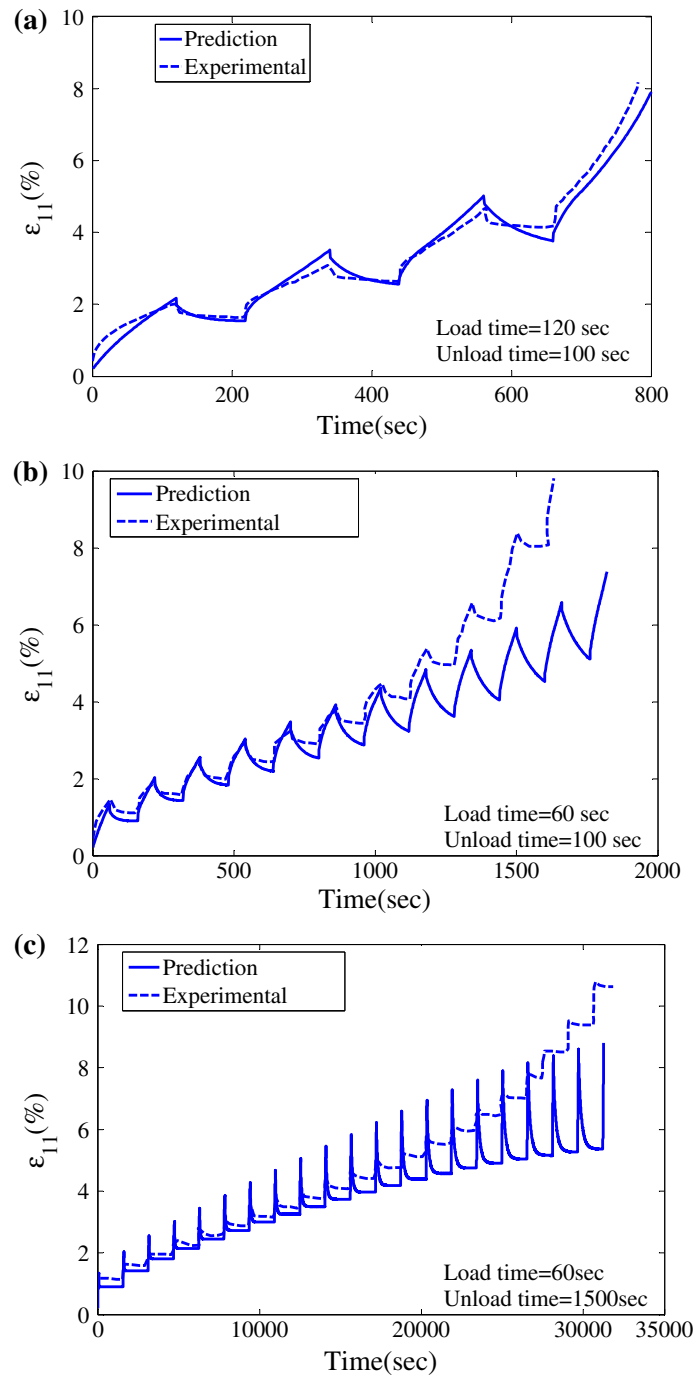


**Fig. 6** Comparison of predicted and experimental multi-cycle creep-recovery response under uniaxial unconfined compressive stress of 1.0 MPa: **a** load time = 120 s and unload time = 100 s, **b** load time = 60 s and unload time = 100 s and **c** load time = 60 s and unload time = 1,500 s

when only damage is included, material tends to recover to the undeformed state; however, when the plasticity is included, the material recovers to a significant residual strain. Figure 9b shows the corresponding evolution of energy densities with time. As the loading is applied, the elastic energy, which is the recoverable work at a given time if the applied stress is removed, shows a jump corresponding to the sudden application of creep load. As creep progresses, the viscous dissipation increases proportional to the creep rate while the dissipation due to damage and plasticity increase as a function of the creep deformation. In the model adopted in this work,

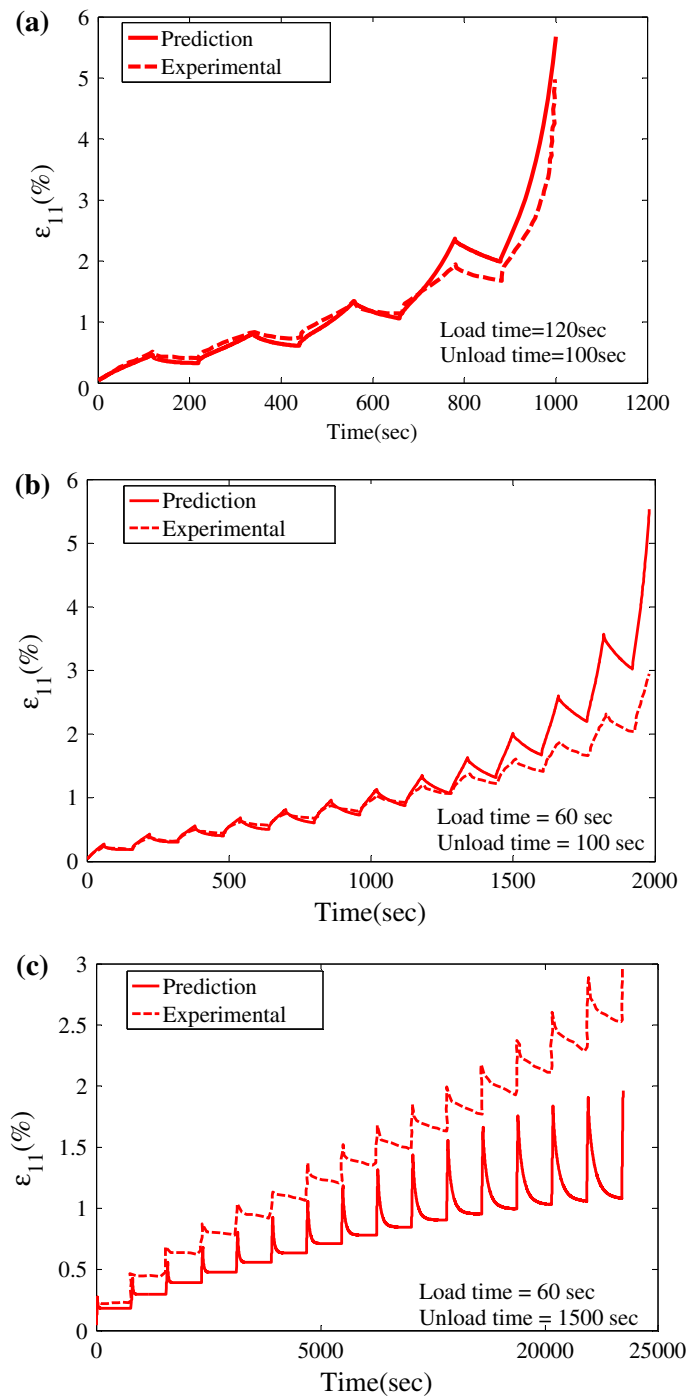


**Fig. 7** Comparison of predicted and experimental multi-cycle creep-recovery response under uniaxial unconfined compressive stress of 0.3 MPa: **a** load time = 120 s and unload time = 100 s, **b** load time = 60 s and unload time = 100 s and **c** load time = 60 s and unload time = 1,500 s

the dissipation due to damage is independent from that due to plasticity and does not change in the absence of plasticity. However, in absence of plasticity, the elastic energy at any time is expectedly larger. Once the stress is removed at 120 s and material is allowed to recover, the elastic energy decreases with time through viscous dissipation as seen from Fig. 9b.

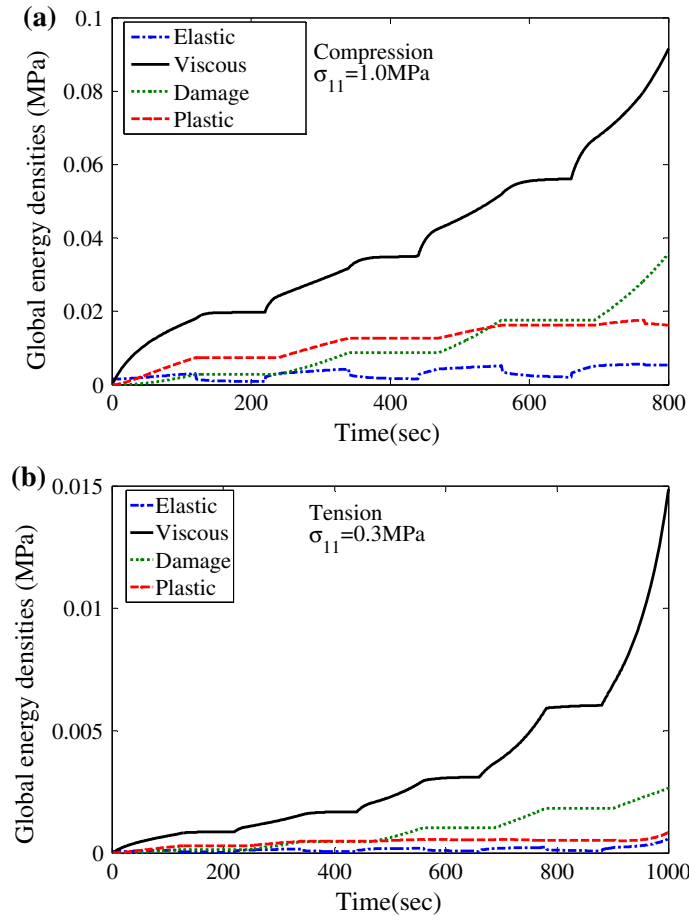


**Fig. 8** Predicted evolution of macro-scale energy densities for the creep-recovery responses shown in Figs. 6a and 7a

During uniaxial creep-recovery, damage evolution in the materials is expected to be anisotropic depending upon the loading direction. To illustrate, how anisotropic damage develops, it is useful to examine the evolution of inter-granular energy densities and damage. Figure 10 shows the inter-granular energy densities in selected orientations as function of time corresponding to the creep-recovery curves in Fig. 9a. We note that the loading is axisymmetric and the inter-granular energy densities are independent of azimuthal angle,  $\phi$ , such that each curve in Fig. 10 refers to  $\theta$  measured with respect to the loading direction-1 (see inset Fig. 10). From Fig. 10, we can see that the inter-granular elastic energies, and viscous, damage and plastic dissipation evolve with time differently in the various directions. Further polar diagrams are given in Fig. 11 that show the evolution of normalized inter-granular energy densities in  $\theta$ -coordinate at selected times. The normalization is again with respect to the total energy in a given orientation, such that the normalized elastic energy, the viscous, the damage and the plastic dissipation densities, denoted by  $r_e$ ,  $r_v$ ,  $r_d$  and  $r_p$  respectively, sum to unity ( $r_e + r_v + r_d + r_p = 1$ ). For the case when only damage is included,  $r_p$  is zero. Also, the evolution of inter-granular damage ( $D_n$  and  $D_w$ ) and normalized plastic displacement ( $\delta_n^{p\alpha}$  and  $\delta_w^{p\alpha}$  normalized with respect to the largest plastic displacement at the end of creep) in the normal and shear directions, respectively, are plotted as polar diagrams at selected times in Fig. 12.

As the loading commences at time  $t = 0$ , the elastic energy fraction  $r_e$  is unity due to sudden loading and viscous, damage and plastic energies fractions are zero as seen in Figs. 10 and 11. As material undergoes creep deformation, the proportions of elastic energies decrease while that of the viscous, damage and plastic (when included) dissipation increases, however, in different ratios in the different directions. Initially at  $t = 5$  s, which is a small fraction of the initial inter-granular retardation time of 57 s, the elastic energy and viscous dissipation are in approximately same proportion in all orientations while both the damage and plastic dissipation is negligibly small. As creep deformation progresses, the proportion of damage and plastic dissipation increases with maximum being in the direction of loading. However, in the orientations orthogonal

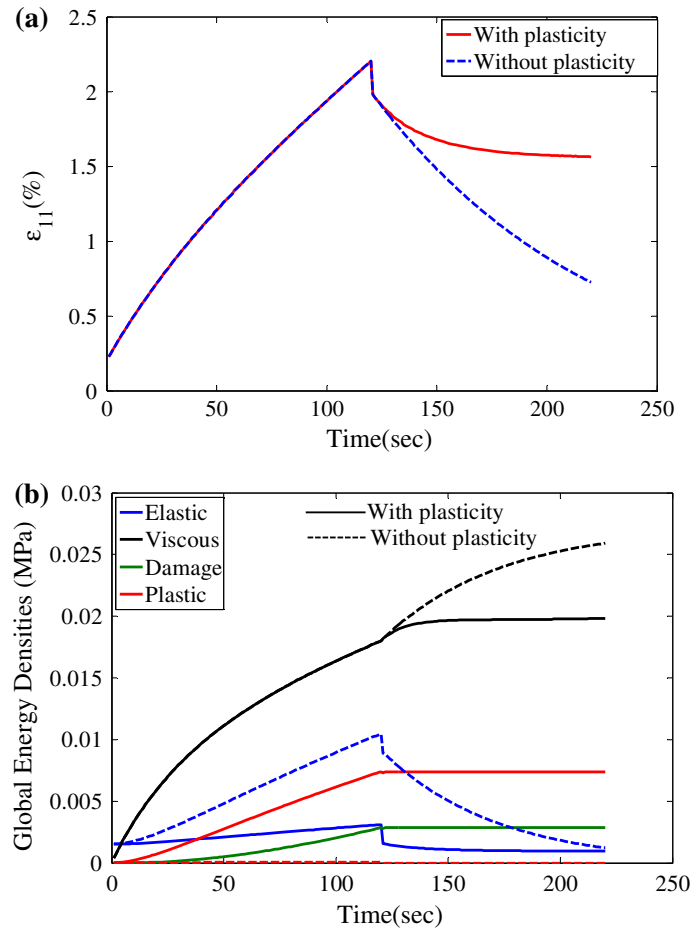


**Fig. 9** **a** Predicted single-cycle creep-recovery response under uniaxial unconfined compressive stress of 1.0MPa for materials with damage only (*dashed curve*) and materials with coupled damage and plasticity (*solid curve*). **b** Predicted evolution of macro-scale energy densities

to loading direction, the proportion of elastic energy remains significantly larger. Beyond the characteristic time of 57s, the proportion of available elastic energy begins to reduce while damage and plastic dissipation increases in all directions, however, in a characteristically orientation-dependent manner. Once again it is notable that load-induced anisotropy provides elastic energy densities whose polar plots no longer exhibit a convex shape, similar to anisotropic elastic materials where a similar lack of convexity is observed [82,83]. Further, a comparison of Fig. 11a, b at  $t = 75$  s shows that in the presence of plastic dissipation the elastic energy is smaller than the case when only damage is present. Clearly at the end of creep at  $t = 12$  s, the plastic dissipation has a significant contribution especially in directions with larger inclination to the loading direction. The concomitant anisotropic development of damage and plastic displacement is seen clearly from the inter-granular damage and plasticity in normal and shear direction shown in Fig. 12. These results indicate that the materials undergoing loading–unloading cycles with fixed stress amplitude will progressively develop induced anisotropy. Such effects that manifest due to granular nature of materials are not easily represented by phenomenological constitutive relationships based upon the concepts of traditional Cauchy mechanics or tensorial damage functions.

### 3.3.4 Effect of induced anisotropy

To illustrate the effect of induced anisotropy, we compare the creep-recovery behavior for a two cycle loading sequence in which the loading direction is changed after the first cycle. The loading sequence is as follows. In case 1, the first cycle load is applied as  $\sigma_{11} = 1.0$ MPa ( $\sigma_{22} = \sigma_{33} = 0$ ) for  $LT = 120$ s,  $UT = 100$ s and the second cycle is kept identical. In case 2, the first cycle is same as that of case 1; however, the second

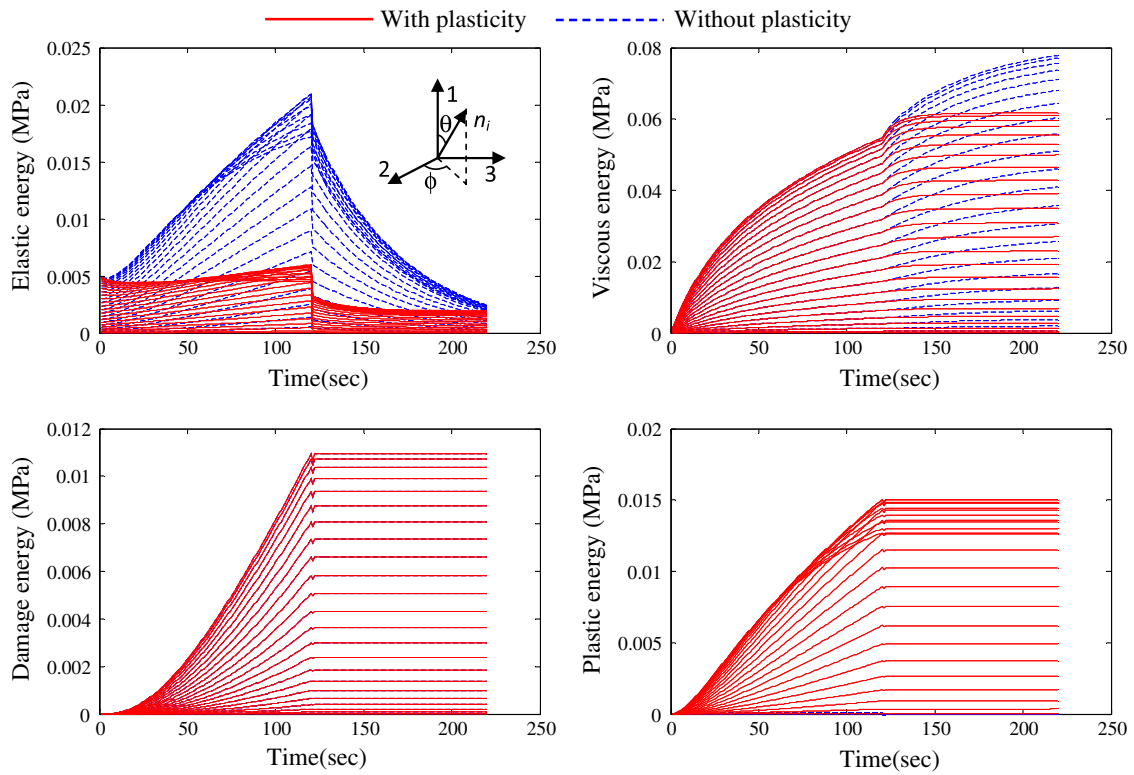


**Fig. 10** Predicted evolution of inter-granular (micro-scale) energy densities with time for the creep-recovery response shown in Fig. 9

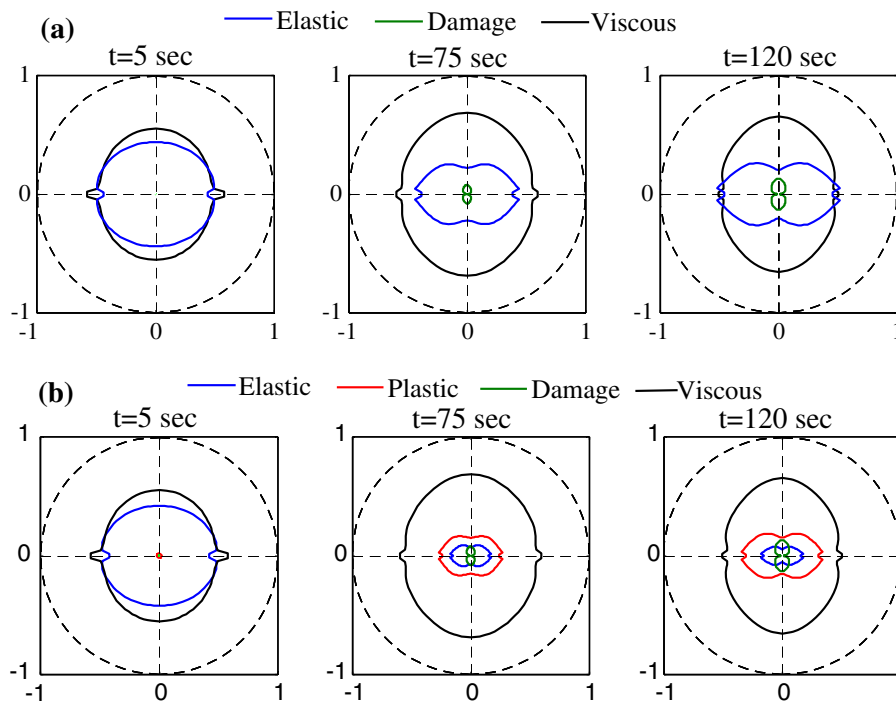


**Fig. 11** Polar plots of inter-granular (micro-scale) energy densities fractions at selected times corresponding to the creep response in Fig. 9

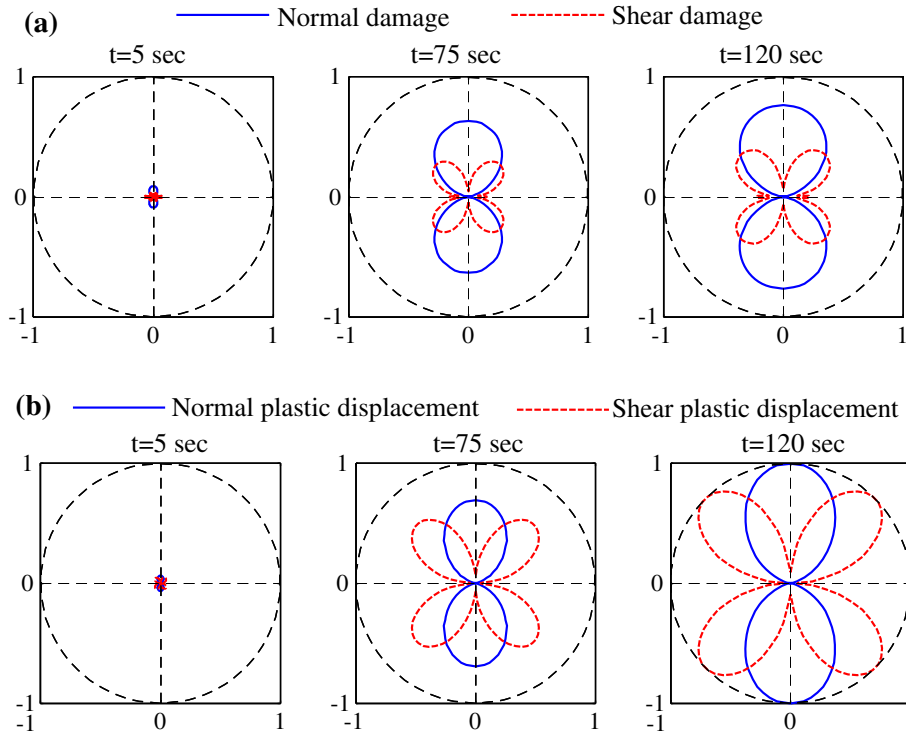


**Fig. 12** Polar plots of inter-granular normal and shear direction **a** damage and **b** normalized plastic displacement at selected times corresponding to the creep response in Fig. 9

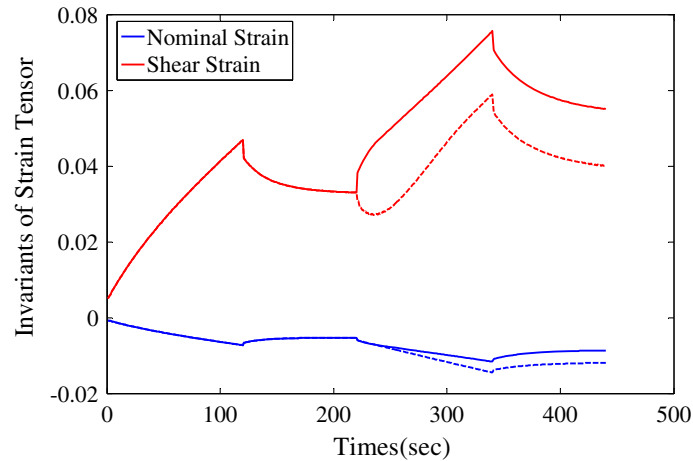


**Fig. 13** Predicted effect of induced anisotropy on a 2-cycle creep-recovery response. The 2nd cycle loading direction is same as the 1st cycle for the *solid curve* while it is orthogonal to the 1st cycle for the *dashed curve*

cycle load is applied as  $\sigma_{22} = 1.0 \text{ MPa}$  ( $\sigma_{11} = \sigma_{33} = 0$ ) for  $LT = 120 \text{ s}$ ,  $UT = 100 \text{ s}$ . For the comparison purpose, we plot in Fig. 13 the nominal strain defined as  $\gamma_n = (\varepsilon_1 + \varepsilon_2 + \varepsilon_3)/3$  and shear strain defined as  $\tau_s = \frac{2}{3} \sqrt{(\varepsilon_1 - \varepsilon_2)^2 + (\varepsilon_2 - \varepsilon_3)^2 + (\varepsilon_3 - \varepsilon_1)^2}$  for the two loading cases. The effect of induced anisotropy is clear from the response. Since the 2-direction has experienced smaller damage and plasticity in the first cycle, the response in the second cycle is stiffer for case 2. In many conventional models that do not incorporate directional evolution of damage tensor and plastic potentials, the material would be treated as isotropic upon recovery. In this case, the second cycle response would have been identical for the two loading cases. While granular materials, in general, are known to exhibit such strong affects of induced anisotropy, experimental data on rate-dependent or creep-recovery response for these materials are scarce (unavailable to our knowledge),

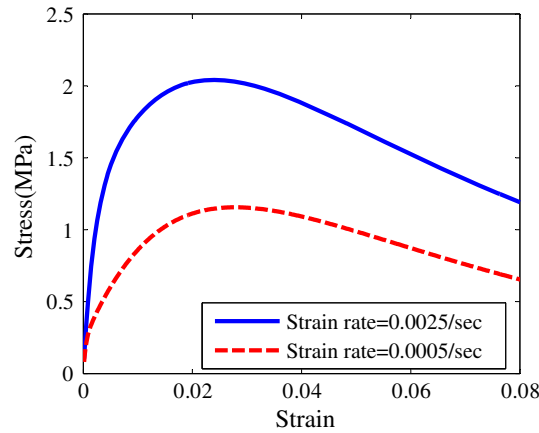


**Fig. 14** Predicted creep curves for hot mix asphalt at two strain rates

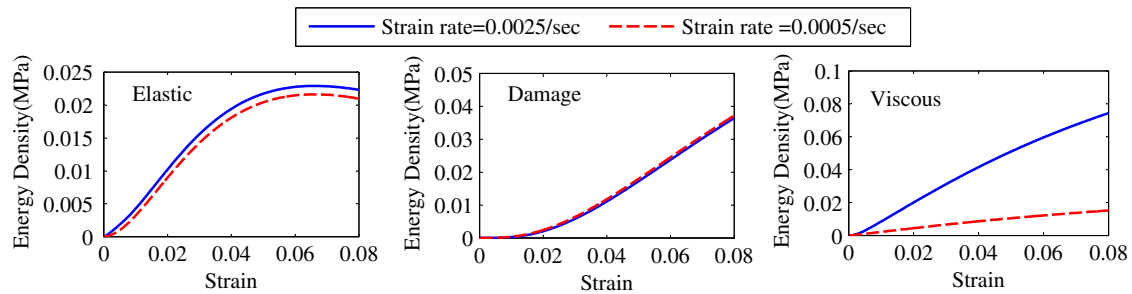


**Fig. 15** Predicted evolution of macro-scale energy densities with strain corresponding to the stress–strain curves given of Fig. 14

especially those that investigate effects of changing loading paths. To that extent, the illustrative calculations discussed here could serve as a basis for systematic investigation into the effect of path dependency of granular material behavior subjected to creep and rate-dependent loading under complex paths.

### 3.3.5 Monotonic behavior

The experimental verification of the model's ability to predict monotonic rate-dependent behavior was shown in our previous paper [10]. The monotonic behavior is investigated for uniaxial unconfined constant strain rate loading applied as follows:  $\varepsilon_{11} = \varepsilon_0 t$ , and lateral stress,  $\sigma_{22} = \sigma_{33} = 0$ . Here, we demonstrate the effect of strain rates,  $\varepsilon_0$ , upon the evolution of energy densities and damage with loading. For our illustrative calculations, we utilize an initial retardation time  $\tau_{n\delta}(0) = 5.7$  s, and use for all other model parameters the same values as those used for creep predictions. For the smaller initial retardation time, the effect of damage on the overall stress–strain behavior is significant at the strain rates for which the simulations have been performed. Predicted stress–strain curves for strain rates of  $\varepsilon_0 = 0.0025/s$  and  $\varepsilon_0 = 0.0005/s$  are given in Fig. 14. With the increase in the strain rate, peak stress increases, whereas the corresponding strains at peak stress decrease. Such behavior is expected for rate-dependent material and indicates that at higher strain rates, the material is stiff, brittle and fails at higher stress. Elastic energy, and viscous and damage densities at two strain rates are shown in Fig. 15. Again, we note that in the absence of unloading, plastic dissipation has not been separately calculated and is contained within elastic energy shown in Fig. 15. Thus, the elastic energy represents partly the amount of recoverable work at a given time if the applied stress is removed and material is unloaded. The elastic energy and damage dissipation show little effect of loading rate for the given set of model parameters; however, with an increase in the loading rate, viscous dissipation appears to be considerably larger.

We further illustrate the evolution of anisotropic dissipation, damage and plasticity with loading by plotting inter-granular energy densities and damage. In Fig. 16, we show the inter-granular energy densities in selected orientations as function of strain for the two strain rates. The normalized fractional inter-granular energy densities are also shown in polar plots in Fig. 17 at selected strains for the two strain rates. As in the case of creep, we can see that the inter-granular elastic energies, and viscous and damage dissipation evolve with strain

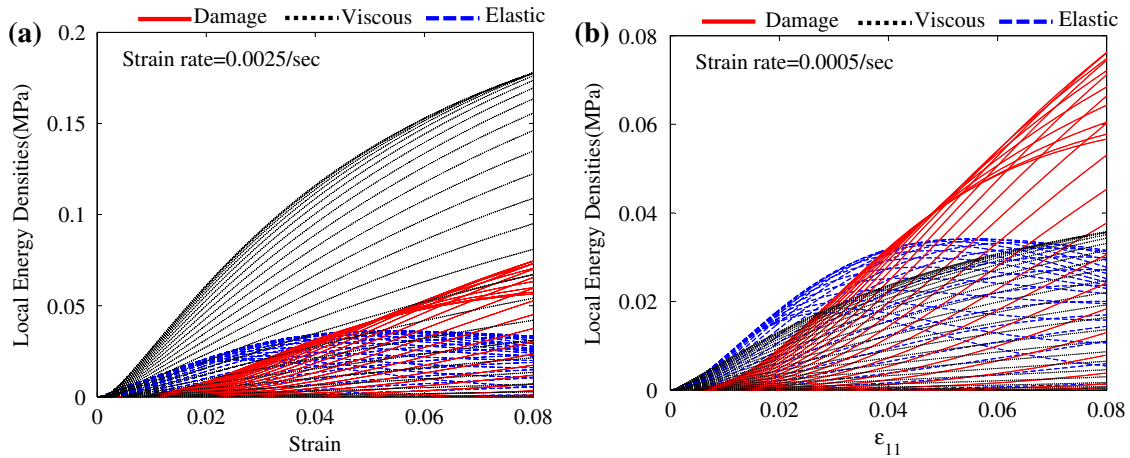


**Fig. 16** Predicted evolution of inter-granular (micro-scale) energy densities with strain under monotonic loading at **a** strain rate = 0.0025/s, and **b** strain rate = 0.0005/s

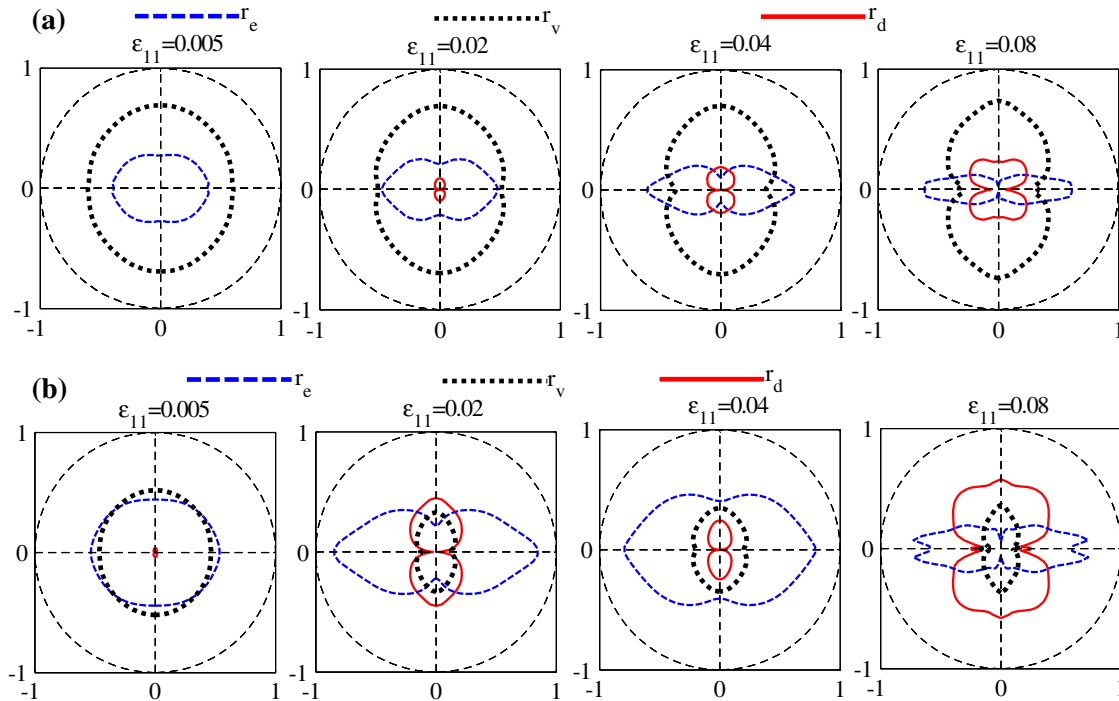


**Fig. 17** Polar plots of inter-granular (micro-scale) energy densities fractions at selected strain levels for the monotonic loading at **a** strain rate = 0.0025/s, and **b** strain rate = 0.0005/s

differently in the various directions; however, we observe that the viscous dissipation is dominant at the higher loading rate. From the polar plots, it is evident that with the increase in strain, damage dissipation fraction,  $r_d$  of the inter-granular contacts oriented in direction of loading increases whereas the corresponding elastic energy fraction,  $r_e$ , decreases. This decrease in  $r_e$  is expected because contacts are undergoing softening process and their capacity to sustain load decreases. We note that in this case as well the load-induced anisotropy leads to elastic energy densities whose polar plots do not exhibit a convex shape, similar to anisotropic elastic materials [82,83]. Finally, the polar plots of inter-granular damage and plastic displacement in normal and shear directions are given in Fig. 18 for the strain rate of 0.0025/s. Similar results are obtained for slower loading rate since the damage dissipation is same for the two loading rates. As in the case of creep loading, these damage and plastic displacement plots show the loading-induced anisotropy in the medium, which will

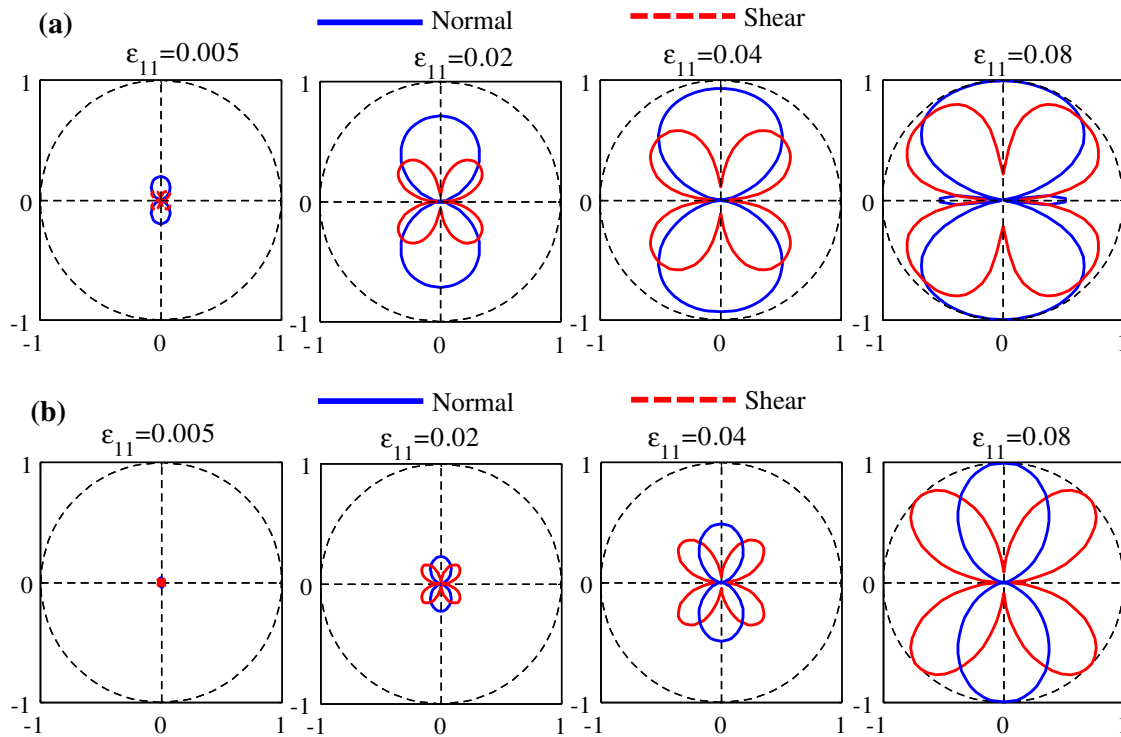


**Fig. 18** Polar plots of inter-granular normal and shear direction **a** damage and **b** normalized plastic displacement at selected strain levels for the monotonic loading at strain rate of 0.0025/s

affect the behavior under multi-axial loading, especially for cases in which the principal loading directions change during the loading process.

### 3.4 Comparison with 3-point bending experiments

The applicability of the developed model is further demonstrated by comparison of model prediction with results of 3-point bending experiments performed on hydrophobic–hydrophilic polymers [84,85]. The application of the current model to these amorphous polymers with ill-defined molecular structure is justified by considering a coarse-grained granular structure at their meso-scales. The experiments were performed on dry and wet environments to obtain the material response under creep and monotonic loading. Creep experiments were performed at a load of 0.3 N, while the monotonic experiments were performed at two loading rates of 60 and 2  $\mu\text{m}/\text{min}$ , respectively. The experimental details are described in our previous work [85]. To simulate the 3-point bending experiments, the derived model was implemented into an Euler-Bernoulli beam framework to predict the nonlinear beam bending. Model parameter identification was performed using the creep results at small times and the monotonic loading results at 60  $\mu\text{m}/\text{min}$ . The following model parameters were found for dry (wet) case:  $G_1 = 0.5E_1$ ,  $G_w = E_n$ ,  $\mu_n = \mu_w$ , and  $B_n = B_w = 10.0 \times 10^{-3}$  where  $E_1 = 6 \text{ GPa/m}$  (3 GPa/m),  $E_n = 10.5 \text{ GPa/m}$  (4.5 GPa/m),  $\tau_{n\delta}(0) = 428 \text{ s}$  (500 s),  $\tau_{nf}(0) = 272 \text{ s}$  (300 s) and  $\beta = 5$ . The results of parameter identification and predicted response at 2  $\mu\text{m}/\text{min}$  are shown in Fig. 19. The discrepancy in the theoretical calculations and experiments in Fig. 19 can be partly attributed to the multiple characteristics time of these complex polymers even under small loads wherein these materials can be treated as linear viscoelastic. Under monotonic loading, the behavior is highly nonlinear as observed from the experimental measurements. The theoretical calculations based upon the model are able to describe the measured nonlinearity reasonably well in both dry and wet conditions. We note that the theoretical calculations of the behavior of wet conditions requires mainly the modification the inter-granular stiffness suggesting that the presence of water softens or plasticizes the inter-granular interactions without changing the strain to reach peak strength indicated by the parameters  $B_n$  and  $B_w$ .

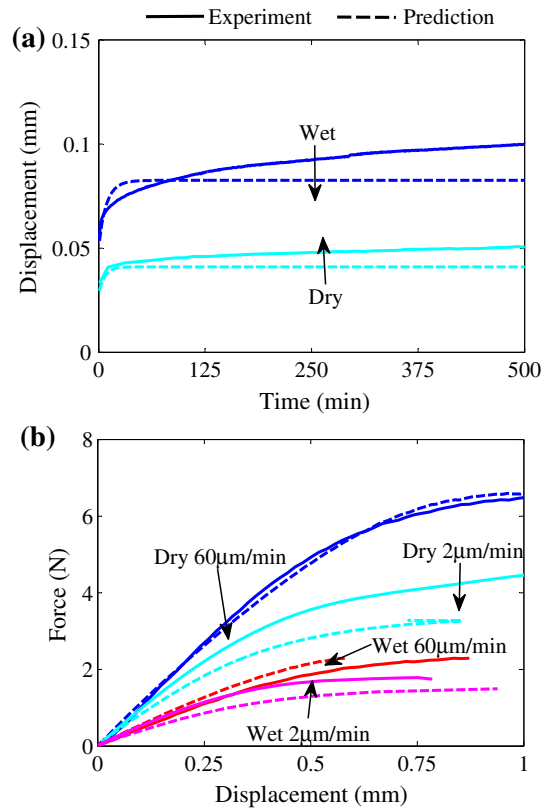


**Fig. 19** Experimental and predicted **a** creep curves at 0.3 N load and **b** load displacement curves for dentin adhesive under dry and wet environment

#### 4 Summary and conclusions

A thermo-mechanical framework for deriving constitutive equations from granular micromechanics approach has been developed. The motivation of the work is to ensure that the derived model for a deforming granular medium satisfies thermodynamic equilibrium at each grain interaction. The framework is then utilized to obtain constitutive equations for nonlinear rate-dependent materials with damage and plasticity. In the developed approach, elastic and dissipation potentials are identified at the micro-scale defined as the inter-granular interactions. The macro-scale Helmholtz free energy and dissipation potential are then obtained as a sum of the micro-scale energies over all the inter-granular interactions in a VE. For rate-dependent damage-plasticity modeling, three internal variables are introduced at the macro-scale to account for the viscous, plastic and damage dissipations. The macro-scale Cauchy stress tensor is then obtained in the usual manner by partial differentiation of overall Helmholtz energy with respect to strain tensor. The resultant expression for stress tensor is found to be a function of inter-granular forces and the relationship of micro-macro kinematical quantities. Further, the application of orthogonality conditions at the macro-scale suggests a Clausius–Duhem type inequality for inter-granular interactions. This inequality can be utilized to establish inter-granular constitutive equations, which along with the expression for Cauchy stress complete the derivation of macro-scale constitutive relationship.

To illustrate the applicability of the model, we have introduced particular choice of inter-granular interactions that include a purely elastic part and a part associated with rate-dependent process that undergoes damage and plasticity. For practical application of the derived model, the macro-scale strain is assumed to be related to the inter-granular displacements using the widely accepted mean field kinematic assumption. The resultant model is implemented in a numerical scheme to predict the creep, creep-recovery and rate-dependent monotonic response of hot-mix asphalt and calculate their associated elastic energy, and viscous, plastic and damage dissipation both at the macro- and micro-scale. The particular inter-granular interactions used in this paper can be extended or modified to account for additional phenomena, such as moisture or heat-related material softening and degradation, further tension-compression asymmetry and normal-shear coupling of dissipation.

The thermo-mechanical framework developed in this work for the granular medium is general in that it only requires the specification of appropriate inter-granular free energy function and dissipation potential. For example, using the developed equations, we can derive thermal properties, such as specific heat capacity, thermal conductivity and thermal expansion coefficients for the granular material systems in terms of the micro-scale quantities. Thus, the approach can be applied to a range of physical or chemical phenomena [86] that effect inter-granular interactions in granular materials. The approach could be particularly useful for elucidating the effects of dissipation in porous media [87,88], higher-gradient and micromorphic continuum theories of granular systems. It is noteworthy that the advantage of the resultant constitutive model is that it can describe loading-induced material anisotropy particularly under evolving multi-axial loading. In classical plasticity and damage mechanics, complex yield criterion, plastic potentials, hardening functions, damage functions and their evolution laws with loading have to be formulated to address this issue. In addition, the model is also able to describe secondary and tertiary creep, creep rupture, accelerated stress relaxation, pressure sensitivity and shear-induced volume change. The mentioned loading-induced anisotropy and rate-dependent characteristics are widely observed for materials such as Portland cement paste, asphalt concrete, frozen soils, cross-linked polymers, sands, glacial sediments, clays and rocks (see for example [89–91]) and are often a manifestation of the granular/discrete nature of materials. In addition, the developed approach can be extended to derive constitutive relations for enhanced continuum models, such as those for higher-gradient or micro-polar theories [33,36,38,39,41], that are necessary for describing phenomena requiring inherent length scales. To this end, we note that the simplifying kinematical assumption used in the present work in which we ignore the particle rotations and higher gradients of displacement leads to the derived classical Cauchy continuum-type theory. In the future, we expect to develop continuum theories that provide a much more complete account of microstructure such as those discussed in [51–54] by systematically relaxing these assumptions.

**Acknowledgments** This research is supported in part by the United States National Science Foundation Grant CMMI-1068528.

## References

1. Pipkin, A.C., Rogers, T.G.: A non-linear integral representation for viscoelastic behaviour. *J. Mech. Phys. Solids* **16**(1), 59–72 (1968). doi:[10.1016/0022-5096\(68\)90016-1](https://doi.org/10.1016/0022-5096(68)90016-1)
2. Wineman, A.: Nonlinear viscoelastic solids—a review. *Math. Mech. Solids* **14**(3), 300–366 (2009). doi:[10.1177/1081286509103660](https://doi.org/10.1177/1081286509103660)
3. Darabi, M.K., Abu Al-Rub, R.K., Masad, E.A., Huang, C.W., Little, D.N.: A thermo-viscoelastic–viscoplastic–viscodamage constitutive model for asphaltic materials. *Int. J. Solids Struct.* **48**(1), 191–207 (2011). doi:[10.1016/j.ijsolstr.2010.09.019](https://doi.org/10.1016/j.ijsolstr.2010.09.019)
4. Lai, J., Bakker, A.: 3-D schapery representation for non-linear viscoelasticity and finite element implementation. *Comput. Mech.* **18**(3), 182–191 (1996). doi:[10.1007/Bf00369936](https://doi.org/10.1007/Bf00369936)
5. Schapery, R.A.: On the characterization of nonlinear viscoelastic materials. *Polym. Eng. Sci.* **9**(4), 295–310 (1969)
6. Schapery, R.A.: Nonlinear viscoelastic solids. *Int. J. Solids and Struct.* **37**(1–2), 359–366 (2000). doi:[10.1016/S0020-7683\(99\)00099-2](https://doi.org/10.1016/S0020-7683(99)00099-2)
7. Green, A.E., Rivlin, R.S.: The mechanics of non-linear materials with memory. *Arch. Ration. Mech. Anal.* **1**(1), 1–21 (1957)
8. Drozdov, A.D.: A constitutive model for nonlinear viscoelastic media. *Int. J. Solids Struct.* **34**(21), 2685–2707 (1997). doi:[10.1016/S0020-7683\(96\)00178-3](https://doi.org/10.1016/S0020-7683(96)00178-3)
9. Abu Al-Rub, R.K., Darabi, M.K.: A thermodynamic framework for constitutive modeling of time- and rate-dependent materials. Part I: theory. *Int. J. Plast.* **34**, 61–92 (2012). doi:[10.1016/j.ijplas.2012.01.002](https://doi.org/10.1016/j.ijplas.2012.01.002)
10. Misra, A., Singh, V.: Micromechanical model for viscoelastic materials undergoing damage. *Contin. Mech. Thermodyn.* **25**(2–4), 343–358 (2013). doi:[10.1007/s00161-012-0262-9](https://doi.org/10.1007/s00161-012-0262-9)
11. Cosserat, E., Cosserat, F.: *Theory of Deformable Bodies*. Scientific Library: A. Hermann And Sons, Paris (1909)
12. Mindlin, R.D.: Micro-structure in linear elasticity. *Arch. Ration. Mech. Anal.* **16**(1), 51–78 (1964)
13. Toupin, R.A.: Theories of elasticity with couple-stress. *Arch. Ration. Mech. Anal.* **17**(2), 85–112 (1964)
14. Eringen, A.C.: *Microcontinuum Field Theories: Foundations and Solids*, vol. 487. Springer, New York (1999)
15. Green, A.E., Rivlin, R.S.: Multipolar continuum mechanics. *Arch. Ration. Mech. Anal.* **17**(2), 113–147 (1964)
16. Germain, P.: Method of virtual power in continuum mechanics. Part 2: microstructure. *Siam J. Appl. Math.* **25**(3), 556–575 (1973). doi:[10.1137/0125053](https://doi.org/10.1137/0125053)
17. Chang, C.S., Misra, A.: Theoretical and experimental-study of regular packings of granules. *J. Eng. Mech. ASCE* **115**(4), 704–720 (1989)
18. Chang, C.S., Misra, A.: Packing structure and mechanical-properties of granulates. *J. Eng. Mech. ASCE* **116**(5), 1077–1093 (1990)
19. Digby, P.J.: The effective elastic moduli of porous granular rocks. *J. Appl. Mech.* **48**, 803–808 (1981)
20. Walton, K.: The effective elastic moduli of a random packing of spheres. *J. Mech. Phys. Solids* **35**, 213–226 (1987)
21. Deresiewicz, H.: Stress–strain relations for a simple model of a granular medium. *J. Appl. Mech.* **25**, 402–406 (1958)
22. Duffy, J., Mindlin, R.D.: Stress–strain relations of a granular medium. *J. Appl. Mech.* **24**(4), 585–593 (1957)
23. Jenkins, J.T.: Volume change in small strain axisymmetric deformations of a granular material. In: Satake, M., Jenkins, J.T. (eds.) *Micromechanics of Granular Materials*, pp. 245–252. Elsevier, Amsterdam (1988)

24. Navier, C.L.: Sur les lois de l'équilibre et du mouvement des corps solides élastiques. *Memoire de l'Academie Royale de Sciences* **7**, 375–393 (1827)
25. Cauchy, A.-L.: Sur l'équilibre et le mouvement d'un système de points matériels sollicités par des forces d'attraction ou de repulsion mutuelle. *Exercices de Mathématiques* **3**, 188–212 (1826–1830)
26. dell'Isola, F., Andreaus, U., Placidi, L.: At the origins and in the vanguard of peri-dynamics, non-local and higher gradient continuum mechanics. An underestimated and still topical contribution of Gabrio Piola. *Mech. Math. Solids* (2013). doi:[10.1177/1081286513509811](https://doi.org/10.1177/1081286513509811)
27. Arndt, M., Griebel, M.: Derivation of higher order gradient continuum models From atomistic models for crystalline solids. *Multiscale Model. Simul.* **4**(2), 531–562 (2005)
28. Blanc, X., Le Bris, C., Lions, P.L.: From molecular models to continuum mechanics. *Cr. Acad. Sci. I Math.* **332**(10), 949–956 (2001)
29. E, W.N., Huang, Z.Y.: A dynamic atomistic-continuum method for the simulation of crystalline materials. *J. Comput. Phys.* **182**(1), 234–261 (2002). doi:[10.1006/jcph.2002.7164](https://doi.org/10.1006/jcph.2002.7164)
30. Chang, C.S., Misra, A., Acheampong, K.: Elastoplastic deformation for particulates with frictional contacts. *J. Eng. Mech. ASCE* **118**(8), 1692–1707 (1992). doi:[10.1061/\(ASCE\)0733-9399\(1992\)118:8\(1692\)](https://doi.org/10.1061/(ASCE)0733-9399(1992)118:8(1692))
31. Chang, C.S., Hicher, P.Y.: An elasto-plastic model for granular materials with microstructural consideration. *Int. J. Solids Struct.* **42**(14), 4258–4277 (2005). doi:[10.1016/j.ijsolstr.2004.09.021](https://doi.org/10.1016/j.ijsolstr.2004.09.021)
32. Chang, C.S., Liao, C.L.: Estimates of elastic modulus for media of randomly packed granules. *Appl. Mech. Rev.* **47**(1), 197–206 (1994)
33. Chang, C.S., Ma, L.: Elastic-material constants for isotropic granular solids with particle rotation. *Int. J. Solids Struct.* **29**(8), 1001–1018 (1992). doi:[10.1016/0020-7683\(92\)90071-Z](https://doi.org/10.1016/0020-7683(92)90071-Z)
34. Misra, A., Chang, C.S.: Effective elastic moduli of heterogeneous granular solids. *Int. J. Solids Struct.* **30**(18), 2547–2566 (1993)
35. Misra, A., Yang, Y.: Micromechanical model for cohesive materials based upon pseudo-granular structure. *Int. J. Solids Struct.* **47**(21), 2970–2981 (2010). doi:[10.1016/j.ijsolstr.2010.07.002](https://doi.org/10.1016/j.ijsolstr.2010.07.002)
36. Alibert, J.J., Seppecher, P., dell'Isola, F.: Truss modular beams with deformation energy depending on higher displacement gradients. *Math. Mech. Solids* **8**(1), 51–73 (2003). doi:[10.1177/108128603029658](https://doi.org/10.1177/108128603029658)
37. dell'Isola, F., Vidoli, S.: Continuum modelling of piezoelectromechanical truss beams: an application to vibration damping. *Arch. Appl. Mech.* **68**(1), 1–19 (1998)
38. Seppecher, P., Alibert, J.-J., dell'Isola, F.: Linear elastic trusses leading to continua with exotic mechanical interactions. *J. Phys. Conf. Ser.* **319**(1), 012018 (2011)
39. Chang, C.S., Askes, H., Sluys, L.J.: Higher-order strain/higher-order stress gradient models derived from a discrete microstructure, with application to fracture. *Eng. Fract. Mech.* **69**(17), 1907–1924 (2002)
40. Yang, Y., Ching, W.-Y., Misra, A.: Higher-order continuum theory applied to fracture simulation of nano-scale intergranular glassy film. *J. Nanomech. Micromech.* **1**(2), 60–71 (2011)
41. Yang, Y., Misra, A.: Micromechanics based second gradient continuum theory for shear band modeling in cohesive granular materials following damage elasticity. *Int. J. Solids Struct.* **49**(18), 2500–2514 (2012). doi:[10.1016/j.ijsolstr.2012.05.024](https://doi.org/10.1016/j.ijsolstr.2012.05.024)
42. Coleman, B.D.: Thermodynamics of materials with memory. *Arch. Ration. Mech. Anal.* **17**(1), 1–46 (1964)
43. Ziegler, H.: *An Introduction to Thermomechanics*. 2nd edn. North-Holland, Amsterdam (1983)
44. Maugin, G.A.: *The Thermomechanics of Plasticity and Fracture*, vol. 7. Cambridge University Press, Cambridge, MA (1992)
45. Maugin, G.A., Drouot, R., Sidoroff, F.: *Continuum Thermomechanics: The Art and Science of Modelling Material Behavior A Volume Dedicated to Paul Germain on the Occasion of His 80th Birthday*, vol. 76. Springer, Berlin (2000)
46. Benoit, H., Decker, D., Duplessix, R., Picot, C., Rempp, P., Cotton, J., Farnoux, B., Jannink, G., Ober, R.: Characterization of polystyrene networks by small-angle neutron scattering. *J. Polym. Sci. Poly. Phys. Ed.* **14**(12), 2119–2128 (1976)
47. Gennes, P.G.De : *Scaling Concepts in Polymer Physics*. Cornell University Press, Ithaca, NY (1979)
48. Hazony, D., Hazony, Y., Katz, J.L., Welsch, G.: Average acoustic pulse dispersion length in condensed matter channels. *Philos. Mag.* **86**(20), 3043–3060 (2006). doi:[10.1080/14786430600664130](https://doi.org/10.1080/14786430600664130)
49. Solar, M., Meyer, H., Gauthier, C., Fond, C., Benzerara, O., Schirrer, R., Baschnagel, J.: Mechanical behavior of linear amorphous polymers: Comparison between molecular dynamics and finite-element simulations. *Phys. Rev. E* **85**(2) (2012). doi:[10.1103/Physreve.85.021808](https://doi.org/10.1103/Physreve.85.021808)
50. Greene, M.S., Li, Y., Chen, W., Liu, W.K.: The archetype-genome exemplar in molecular dynamics and continuum mechanics. *Comput. Mech.*, 1–51 (2013). doi:[10.1007/s00466-013-0925-9](https://doi.org/10.1007/s00466-013-0925-9)
51. Ghiba, I.-D., Neff, P., Madeo, A., Placidi, L., Rosi, G.: The relaxed linear micromorphic continuum: existence, uniqueness and continuous dependence in dynamics. *Mathematics and Mechanics of Solids*, arXiv preprint arXiv:1308.3762 (2013). doi:[10.1177/1081286513516972](https://doi.org/10.1177/1081286513516972)
52. Madeo, A., Neff, P., Ghiba, I.-D., Placidi, L., Rosi, G.: Wave propagation in relaxed micromorphic continua: modeling metamaterials with frequency band-gaps. *Contin. Mech. Thermodyn.*, 1–20 (2013). doi:[10.1007/s00161-013-0329-2](https://doi.org/10.1007/s00161-013-0329-2)
53. Neff, P., Ghiba, I.-D., Madeo, A., Placidi, L., Rosi, G.: A unifying perspective: the relaxed linear micromorphic continuum. *Contin. Mech. Thermodyn.*, 1–43 (2013). doi:[10.1007/s00161-013-0322-9](https://doi.org/10.1007/s00161-013-0322-9)
54. Del Vescovo, D., Giorgio, I.: Dynamic problems for metamaterials: review of existing models and ideas for further research. *Int. J. Eng. Sci.* (2014). doi:[10.1016/j.ijengsci.2014.02.022](https://doi.org/10.1016/j.ijengsci.2014.02.022)
55. Houlsby, G.T., Puzrin, A.M.: A thermomechanical framework for constitutive models for rate-independent dissipative materials. *Int. J. Plast.* **16**(9), 1017–1047 (2000). doi:[10.1016/S0749-6419\(99\)00073-X](https://doi.org/10.1016/S0749-6419(99)00073-X)
56. dell'Isola, F., Seppecher, P., Madeo, A.: How contact interactions may depend on the shape of Cauchy cuts in Nth gradient continua: approach “à la D’Alembert”. *Zeitschrift für Angewandte Mathematik Und Physik* **63**(6), 1119–1141 (2012). doi:[10.1007/s00033-012-0197-9](https://doi.org/10.1007/s00033-012-0197-9)
57. Seppecher, P.: Second-gradient theory: application to Cahn–Hilliard fluids. In: *Continuum Thermomechanics*, pp. 379–388. Springer, Berlin (2002)
58. Magoarić, H., Danescu, A., Cambou, B.: Nonlocal orientational distribution of contact forces in granular samples containing elongated particles. *Acta Geotech.* **3**, 49–60 (2008)

59. Houslsby, G.T., Puzrin, A.M.: Principles of Hyperplasticity: An Approach to Plasticity Theory Based on Thermodynamic Principles. Springer, Berlin (2006)
60. Abu Al-Rub, R.K., Voyiadjis, G.Z.: On the coupling of anisotropic damage and plasticity models for ductile materials. *Int. J. Solids Struct.* **40**(11), 2611–2643 (2003). doi:[10.1016/S0020-7683\(03\)00109-4](https://doi.org/10.1016/S0020-7683(03)00109-4)
61. Einav, I., Houslsby, G.T., Nguyen, G.D.: Coupled damage and plasticity models derived from energy and dissipation potentials. *Int. J. Solids Struct.* **44**(7–8), 2487–2508 (2007). doi:[10.1016/j.ijsolstr.2006.07.019](https://doi.org/10.1016/j.ijsolstr.2006.07.019)
62. Marottide Sciarra, F.: Hardening plasticity with nonlocal strain damage. *Int. J. Plast.* **34**, 114–138 (2012)
63. Voyiadjis, G.Z., Abu Al-Rub, R.K., Palazotto, A.N.: Thermodynamic framework for coupling of non-local viscoplasticity and non-local anisotropic viscodamage for dynamic localization problems using gradient theory. *Int. J. Plast.* **20**(6), 981–1038 (2004). doi:[10.1016/j.ijplas.2003.10.002](https://doi.org/10.1016/j.ijplas.2003.10.002)
64. Carcaterra, A.: Ensemble energy average and energy flow relationships for nonstationary vibrating systems. *J. Sound Vib.* **288**(3), 751–790 (2005). doi:[10.1016/j.jsv.2005.07.015](https://doi.org/10.1016/j.jsv.2005.07.015)
65. Carcaterra, A., Akay, A.: Theoretical foundations of apparent-damping phenomena and nearly irreversible energy exchange in linear conservative systems. *J. Acoust. Soc. Am.* **121**(4), 1971–1982 (2007). doi:[10.1121/1.2697030](https://doi.org/10.1121/1.2697030)
66. Culla, A., Sestieri, A., Carcaterra, A.: Energy flow uncertainties in vibrating systems: definition of a statistical confidence factor. *Mech. Syst. Signal. Process.* **17**(3), 635–663 (2003). doi:[10.1006/mssp.2002.1487](https://doi.org/10.1006/mssp.2002.1487)
67. Rinaldi, A., Krajcinovic, D., Peralta, P., Lai, Y.C.: Lattice models of polycrystalline micro structures: a quantitative approach. *Mech. Mater.* **40**(1–2), 17–36 (2008). doi:[10.1016/j.mechmat.2007.02.005](https://doi.org/10.1016/j.mechmat.2007.02.005)
68. Rinaldi, A., Lai, Y.C.: Statistical damage theory of 2D lattices: energetics and physical foundations of damage parameter. *Int. J. Plast.* **23**(10–11), 1796–1825 (2007). doi:[10.1016/j.ijplas.2007.03.005](https://doi.org/10.1016/j.ijplas.2007.03.005)
69. Rinaldi, A.: Bottom-up modeling of damage in heterogeneous quasi-brittle solids. *Contin. Mech. Thermodyn.* **25**(2–4), 359–373 (2013). doi:[10.1007/s00161-012-0265-6](https://doi.org/10.1007/s00161-012-0265-6)
70. Shim, J., Mohr, D.: Rate dependent finite strain constitutive model of polyurea. *Int. J. Plast.* **27**(6), 868–886 (2011). doi:[10.1016/j.ijplas.2010.10.001](https://doi.org/10.1016/j.ijplas.2010.10.001)
71. Mohr, D.: Mechanism-based multi-surface plasticity model for ideal truss lattice materials. *Int. J. Solids Struct.* **42**(11), 3235–3260 (2005)
72. Chang, C.S., Misra, A.: Application of uniform strain theory to heterogeneous granular solids. *J. Eng. Mech. ASCE* **116**(10), 2310–2328 (1990). doi:[10.1061/\(ASCE\)0733-9399\(1990\)116:10\(2310\)](https://doi.org/10.1061/(ASCE)0733-9399(1990)116:10(2310))
73. Clausius, R.: XVI. On a mechanical theorem applicable to heat. *Lond. Edinb. Dublin Philos. Mag. J. Sci.* **40**(265), 122–127 (1870)
74. Swenson, R.J.: Comments on virial theorems for bounded systems. *Am. J. Phys.* **51**(10), 940–942 (1983). doi:[10.1119/1.13390](https://doi.org/10.1119/1.13390)
75. Irving, J.H., Kirkwood, J.G.: The statistical mechanical theory of transport processes. IV. The equations of hydrodynamics. *J. Chem. Phys.* **18**(6), 817–829 (1950). doi:[10.1063/1.1747782](https://doi.org/10.1063/1.1747782)
76. Tsai, D.H.: Virial theorem and stress calculation in molecular-dynamics. *J. Chem. Phys.* **70**(3), 1375–1382 (1979). doi:[10.1063/1.437577](https://doi.org/10.1063/1.437577)
77. Subramanian, A.K., Sun, C.T.: Continuum interpretation of virial stress in molecular simulations. *Int. J. Solids Struct.* **45**(14–15), 4340–4346 (2008). doi:[10.1016/j.ijsolstr.2008.03.016](https://doi.org/10.1016/j.ijsolstr.2008.03.016)
78. Zhou, M.: A new look at the atomic level virial stress: on continuum-molecular system equivalence. *Proc. R. Soc. Math. Phys. Eng. Sci.* **459**(2037), 2347–2392 (2003). doi:[10.1098/rspa.2003.1127](https://doi.org/10.1098/rspa.2003.1127)
79. Contrafatto, L., Cuomo, A.: A globally convergent numerical algorithm for damaging elasto-plasticity based on the multiplier method. *Int. J. Numer. Methods Eng.* **63**(8), 1089–1125 (2005). doi:[10.1002/Nme.1235](https://doi.org/10.1002/Nme.1235)
80. Contrafatto, L., Cuomo, M.: A new thermodynamically consistent continuum model for hardening plasticity coupled with damage. *Int. J. Solids Struct.* **39**(25), 6241–6271 (2002). doi:[10.1016/S0020-7683\(02\)00470-5](https://doi.org/10.1016/S0020-7683(02)00470-5)
81. Misra, A., Singh, V.: Nonlinear granular micromechanics model for multi-axial rate-dependent behavior. *Int. J. Solids Struct.* (2014). doi:[10.1016/j.ijsolstr.2014.02.034](https://doi.org/10.1016/j.ijsolstr.2014.02.034)
82. Cazzani, A., Rovati, M.: Extrema of Young’s modulus for cubic and transversely isotropic solids. *Int. J. Solids Struct.* **40**(7), 1713–1744 (2003). doi:[10.1016/S0020-7683\(02\)00668-6](https://doi.org/10.1016/S0020-7683(02)00668-6)
83. Cazzani, A., Rovati, M.: Extrema of Young’s modulus for elastic solids with tetragonal symmetry. *Int. J. Solids Struct.* **42**(18–19), 5057–5096 (2005). doi:[10.1016/j.ijsolstr.2005.02.018](https://doi.org/10.1016/j.ijsolstr.2005.02.018)
84. Singh, V., Misra, A., Marangos, O., Park, J., Ye, Q., Kieweg, S.L., Spencer, P.: Viscoelastic and fatigue properties of model methacrylate-based dentin adhesives. *J. Biomed. Mater. Res. B Appl. Biomater.* **95**(2), 283–290 (2010). doi:[10.1002/jbm.b.31712](https://doi.org/10.1002/jbm.b.31712)
85. Singh, V., Misra, A., Parthasarathy, R., Ye, Q., Park, J., Spencer, P.: Mechanical properties of methacrylate-based model dentin adhesives: effect of loading rate and moisture exposure. *J. Biomed. Mater. Res. B Appl. Biomater.* **101**(8), 1437–1443 (2013). doi:[10.1002/jbm.b.32963](https://doi.org/10.1002/jbm.b.32963)
86. Misra, A., Parthasarathy, R., Singh, V., Spencer, P.: Micro-poromechanics model of fluid-saturated chemically active fibrous media. *ZAMM J. Appl. Math. Mech./Zeitschrift für Angewandte Mathematik und Mechanik* (2013). doi:[10.1002/zamm.201300071](https://doi.org/10.1002/zamm.201300071)
87. Madeo, A., dell’Isola, F., Darve, F.: A continuum model for deformable, second gradient porous media partially saturated with compressible fluids. *J. Mech. Phys. Solids* **61**(11), 2196–2211 (2013). doi:[10.1016/j.jmps.2013.06.009](https://doi.org/10.1016/j.jmps.2013.06.009)
88. Madeo, A., George, D., Remond, Y.: Second-gradient models accounting for some effects of microstructure on remodelling of bones reconstructed with bioresorbable materials. *Comput. Methods Biomech.* **16**, 260–261 (2013). doi:[10.1080/10255842.2013.815856](https://doi.org/10.1080/10255842.2013.815856)
89. Kuhn, M.R., Mitchell, J.K.: New perspectives on soil-creep. *J. Geotech. Eng. ASCE* **119**(3), 507–524 (1993)
90. Lade, P.V., Liggio, C.D., Nam, J.: Strain rate, creep, and stress drop-creep experiments on crushed coral sand. *J. Geotech. Geoenviron. Eng.* **135**(7), 941–953 (2009). doi:[10.1061/\(ASCE\)GT.1943-5606.0000067](https://doi.org/10.1061/(ASCE)GT.1943-5606.0000067)
91. Zhou, X.P., Yang, H.Q., Zhang, Y.X.: Rate dependent critical strain energy density factor of Huanglong limestone. *Theor. Appl. Fract. Mech.* **51**(1), 57–61 (2009). doi:[10.1016/j.tafmec.2009.01.001](https://doi.org/10.1016/j.tafmec.2009.01.001)

Reproduced with permission of the copyright owner. Further reproduction prohibited without permission.